The Regional Particulate Matter Model. 1. Model description and preliminary results

Article *in* Journal of Geophysical Research Atmospheres · December 1995

DOI: 10.1029/95JD02093

2 authors:

Francis Binkowski
University of North Carolina at Chapel Hill
84 PUBLICATIONS **6,178** CITATIONS

SEE PROFILE

Uma Shankar
United States Environmental Protection Agency
32 PUBLICATIONS **2,589** CITATIONS

SEE PROFILE

JOURNAL OF GEOPHYSICAL RESEARCH, VOL. 100, NO. D12, PAGES 26,191–26,209, DECEMBER 20, 1995

The Regional Particulate Matter Model
1. Model description and preliminary results

Francis S. Binkowski[1]

Atmospheric Sciences Modeling Division, Air Resources Laboratory, National Oceanic and Atmospheric Administration, Research Triangle Park, North Carolina

Uma Shankar

MCNC, Research Triangle Park, North Carolina

Abstract. The Regional Acid Deposition Model has been modified to create the Regional Particulate Model, a three-dimensional Eulerian model that simulates the chemistry, transport, and dynamics of sulfuric acid aerosol resulting from primary emissions and the gas phase oxidation of sulfur dioxide. The new model uses a bimodal lognormal distribution to represent particles in the submicrometer size range. In addition to including the horizontal and vertical advection and vertical diffusion of the aerosol number concentration and sulfate mass concentration fields, the model now explicitly treats the response of the distribution parameters to particle coagulation within and between the modes, condensation of sulfate vapor onto existing particles, formation of new particles, evaporation and condensation of ambient water vapor in the presence of ammonia, and particle-size-dependent dry deposition. The model has been used to study how the degree of sulfuric acid neutralization by ambient ammonia affects the total aerosol concentrations and particle size distributions over eastern North America. Preliminary results for three representative locations, rural, near-source, and nominal downwind of source, show that the effect is greatest for the rural and smallest for the near-source regions, which corresponds with the largest and smallest values, respectively, of ammonium-to-sulfate molar ratios. The results indicate that the model could provide a tool for investigating the effects of various pollution control strategies, as well as new or alternative formulations of important aerosol processes.

1. Introduction

Particulate matter in the atmosphere can affect the quality of our lives significantly because of its potential impact on human health and the environment. Aerosol particles in the submicrometer size range can be inhaled and thus may pose certain health hazards. Because particles in this size range also scatter light, they strongly influence the radiative budget of the Earth-atmosphere system; they also reduce visibility and diminish the recreational value of national parks and other remote locations. Several surveys of the current state of knowledge of atmospheric aerosols [*Finlayson-Pitts and Pitts*, 1986; *Seinfeld*, 1986; *Warneck*, 1988] point toward a consensus that most submicrometer particles are formed by gas-to-particle conversion processes in the atmosphere. Further, in the eastern half of North America, this size range appears to be dominated by sulfates. Passage of the Clean Air Act of 1990 created strong interest in the mathematical modeling of how atmospheric aerosols behave and their relationship to both natural and anthropogenic sources of sulfur and other species. The Regional Particulate Model (RPM) is being developed as a tool to investigate this relationship.

There have been several recent regional and subregional studies of aerosol production and transport using numerical models. *Russell et al.* [1983, 1985] used a trajectory model to characterize the nitrate aerosol in the Los Angeles area; their work, however, did not include simulation of aerosol size distributions. *Pilinis and Seinfeld* [1987] have published results from a three-dimensional Eulerian photochemical gas-aerosol model for the South Coast Air Basin of California, discussing the aerosol chemistry in three broad-size sections. Using a three-dimensional model developed by *Toon et al.* [1988], *Westphal et al.* [1988] described the transport of Saharan dust. They used 30 sections to represent the size distribution but did not consider particle coagulation. Because the particles of interest were larger than the fine-particle range, the researchers found that coagulation did not alter the size distribution for the cases simulated. *Giorgi* [1986] developed the Atmospheric Aerosol Model for including aerosol dynamics in the National Center for Atmospheric Research Community Climate Model. His work used analytic size distributions (called modes) similar to the RPM's but considered coagulation only within the modes, not between them. *Kötz* [1991] and *Kötz et al.* [1991] used the European Acid Deposition model (EURAD), a version of the Regional Acid Deposition Model (RADM), to develop a model similar to the RPM but without aerosol size distributions. The Denver Air Quality Model (DAQM), another extension of the RADM, also includes only aerosol par-

[1]On assignment to the U.S. Environmental Protection Agency, National Exposure Research Laboratory, Research Triangle Park, North Carolina.

Paper number 95JD02093.
0148-0227/95/95JD-02093$05.00

ticle mass but contains many more species. It is being applied over an urban domain with a grid resolution of about 8 km [*Middleton*, 1993].

In this contribution we describe the model's main characteristics and current status. We then discuss the response of the sulfate aerosol water fraction (defined as the ratio of water to total aerosol mass, namely, sulfate plus ammonium plus water) to neutralization by ammonia. Finally, we discuss future work. In part 2 (F. S. Binkowski and U. Shankar, manuscript in preparation, 1995) we intend to present results from simulations using a new scheme for accounting for cloud scavenging and wet deposition of aerosol particle distributions.

2. Model Description

Using experience gained during the National Acid Precipitation Assessment Program (NAPAP) [*Binkowski et al.*, 1990], we designed the RPM utilizing the gas phase chemistry and transport mechanisms of the RADM, a comprehensive, three-dimensional, Eulerian air quality model [*Chang et al.*, 1990]. The RPM includes not only all of the RADM mechanisms but also the chemistry, transport, and dynamics of aerosol particles [*Shankar and Binkowski*, 1992]. The governing equation of the RADM is the conservation equation for the chemical concentration, C_l, of species l:

$$\frac{\partial C_l^*}{\partial t} = -\nabla \cdot (\mathbf{V} C_l^*) - \frac{\partial}{\partial \sigma}(\dot{\sigma} C_l^*) + \left(\frac{\partial C_l^*}{\partial t}\right)_{\text{Diff}} + \left(\frac{\partial C_l^*}{\partial t}\right)_{\text{Chem}} \tag{1a}$$

$$\left(\frac{\partial C_l^*}{\partial t}\right)_{\text{Chem}} = (R_l P^*)\{P_l - L_l C_l + A_{wl} - D_{wl} + E_l\} \tag{1b}$$

$$C_l^* = (R_l P^*) C_l \tag{1c}$$

where the symbols are defined in the notation section.

The first two terms on the right-hand side of (1a) represent the horizontal and vertical advection of the species concentration by the wind field. The third term represents vertical turbulent transport. For convective conditions, the model uses the Asymmetric Convective Model (ACM) of *Pleim and Chang* [1991]; for other atmospheric conditions, it uses a K theory approach due to *Hass et al.* [1991] (see also *Byun* [1990, 1991]). The fourth term represents production or loss of the species due to chemical reactions, wet deposition, and direct input from emission sources. These are given explicitly in (1b), where the right-hand side terms in the braces are, from left to right, the rates of gas phase production, gas phase loss, aqueous phase production, wet deposition, and source emission for species l. The term in the parentheses converts the concentration from molar mixing ratio to mass mixing ratio multiplied by P^*, as required for transport in the σ coordinate system [*Chang et al.*, 1990]. Dry deposition is represented in the model as a boundary condition on the finite-difference form of the vertical turbulent-transport term. Note that because this is a regional-scale model with horizontal grid spacing of 80 km in the present version, turbulent transport is accounted for only in the vertical direction.

2.1. Aerosol Chemistry

Atmospheric sulfate aerosol is produced when hydroxyl radicals oxidize SO_2 in the presence of water vapor to yield H_2SO_4, which either nucleates or condenses on existing particles, depending upon its concentration [*Middleton and Kiang*, 1978]. Nitrate aerosol production also increases aerosol mass. HNO_3 vapor is a by-product formed during the photochemical production of ozone. If sufficient NH_3 is present in the atmosphere, the H_2SO_4 may be neutralized to $(NH_4)_2SO_4$, and any residual NH_3 may then combine with the HNO_3 to form NH_4NO_3 aerosol. The chemistry of the NH_3-H_2SO_4-HNO_3-H_2O system is treated in the RPM by a modification of the Model for an Aerosol Reacting System (MARS) of *Saxena et al.* [1986].

MARS is an equilibrium model based on fundamental thermodynamics. To minimize the number of equations to be solved, the treatment of chemical and interfacial equilibria focuses only on major species for each given set of ambient conditions. The species treated in the MARS include HNO_3, NH_3, and H_2O in the gas or vapor phase; SO_4^{2-}, HSO_4^-, NH_4^+, NO_3^-, H^+, and H_2O in the liquid phase; and H_2SO_4, with its increasingly neutralized ammonium salts such as NH_4HSO_4 and $(NH_4)_2SO_4$, and HNO_3 with its neutralized salt NH_4NO_3, in the aerosol phase. Not all of these species may be present in a particular aerosol-gas equilibrium. The relative proportions of the species present are dictated by the ratio of NH_4^+ to SO_4^{2-} (i.e., the degree of neutralization of aqueous H_2SO_4), relative humidity, and temperature. For example, for a given set of concentrations, the aerosol may be a liquid or a solid; and for another, the aqueous phase may be devoid of NO_3^-. Another important consideration is the relative humidity of deliquescence for the sulfate and nitrate salts.

The distinguishing feature of the original formulation of MARS is its division of the entire regime of aerosol species into several subdomains in ambient relative humidity and the molar ratio of NH_4^+ to SO_4^{2-}. While we have retained its basic structure, we have completely revised the data used in calculating the liquid water content (LWC) of the aerosol. In calculating the LWC, we assume that an ambient aerosol over the eastern portions of the United States and southern Canada is most probably in the metastable state (aqueous droplets), that is, the relative humidity is greater than that for crystallization but less than that for deliquescence [*Rood et al.*, 1989; *Spann and Richardson*, 1985]. Thus we have ignored the effects of deliquescence and hysteresis for aerosol adjustment to relative humidity. Our argument for this is that when H_2SO_4 is formed through the oxidation of SO_2 by hydroxyl radicals, the process always occurs in the presence of water vapor. This H_2SO_4 solution is hygroscopic and adjusts very quickly to the ambient relative humidity, leading to an aqueous aerosol droplet, whether by direct nucleation or by condensation upon an existing particle. NH_3 molecules then bombard the aerosol particle, and the process of neutralization commences. This process differs from the laboratory system, in which a dry ammonium salt particle is humidified to deliquescence and a solution droplet is formed. *Spann and Richardson*'s [1985] experiment represents part of this process by beginning with NH_4HSO_4 and adding more NH_3 to further neutralize the sulfate. However, they reduced the relative humidity low enough for crystallization to occur. In the atmosphere, neutralization takes place under ambient conditions. The main point is that unless the atmospheric relative humidity is lowered to that of crystallization, the particle remains liquid during the entire neutralization process.

To illustrate this point further, at night with a surface-based temperature inversion, vertical transport of NH_3 (emitted from the ground surface) is inhibited, and surface-layer concentra-

tions can increase with time. This increase means that the probability of an NH_3 molecule striking an aerosol particle is enhanced, leading to further neutralization. During this period of falling temperatures, relative humidity increases. During the day, when photochemical oxidation of SO_2 leads to H_2SO_4 formation, NH_3 is transported over the much deeper surface-based mixing layer, and the probability of neutralization is diminished. Relative humidity decreases during the day, but the aerosols in the surface-based mixing layer are also transported, and as they rise they encounter decreasing temperatures with increasing relative humidity. We would thus expect crystallization to occur only under very arid conditions. Hence we assume that the aerosols are always in a wetted state when relative humidities are greater than that for crystallization.

In order to calculate the aerosol LWC, we used a fit to the experimental water activities reported by *Spann and Richardson* [1985] for H_2O-to-SO_4^{2-} molar ratios as a function of the NH_4^+-to-SO_4^{2-} molar ratio. For water activities greater than those given by *Spann and Richardson* [1985], we used the experimental results from *Nair and Vohra* [1975], *Tang* [1980], and *Cohen et al.* [1987]. Thus we fit the entire range of relative humidity (water activity) from crystallization to near 100%.

Currently, we follow the MARS paradigm that all ambient NH_3 is converted to NH_4^+ up to an NH_4^+-to-SO_4^{2-} molar ratio of 2.0 (fully neutralized sulfate). Whereas this is likely to be a good approximation for molar ratios of 1.5 or less, the results of *Spann and Richardson* [1985] show that the approach to full neutralization by the addition of NH_3 may slow down for molar ratios closer to 2.0. In particular, their results show that the crystallization curve does not approach the same value of relative humidity as their own previous work [*Richardson and Spann*, 1984]. *Aurian-Blajeni et al.* [1992] and *Koutrakis and Aurian-Blajeni* [1993] also have presented data showing incomplete neutralization of sulfuric acid for molar ratios between 1.9 and 2.0. Furthermore, *Harrison and Kitto* [1992] report that atmospheric observations show a reduction in the rate constant with acidic sulfate with decreasing aerosol acidity for the reaction of ammonium. *Seinfeld* [1986] shows that $[NH_4^+]$ is an increasing function of $[H^+]$, that is, the more acidic the solution, the more NH_3 goes into solution. As a consequence, our current rates of neutralization of H_2SO_4 are likely to be overestimates for the near-neutralized aerosols.

Finally, the MARS paradigm is based upon a molal (moles of solute per kilogram of water) concentration scale, which becomes increasingly inaccurate as aerosol LWC decreases with decreasing relative humidity. Recent work of *Clegg et al.* [1992] and *Clegg and Pitzer* [1992] argues for a mole fraction concentration scale that extends the molal ion interaction model of *Pitzer* [1987, 1991] to very low humidities and to fused aerosol particles. We intend to incorporate these advances into the RPM in the future. Also, for the work presented here we assumed that the aerosol consists entirely of SO_4^{2-}, NH_4^+, and H_2O. This simplified system was used as a model development platform. Consequently, we have considered neither nitrates nor organic and elemental carbon components. As we improve the aerosol phase chemistry of the model, these additional species will be included.

2.2. Aerosol Dynamics

The aerosol particle size distribution is modeled upon the concepts developed by *Whitby* [1978]. The particles are divided into two size ranges, or modes. The smaller (nuclei) mode represents fresh emissions, while the larger (accumulation) mode represents aged particles. The particle dynamics of this aerosol distribution are described fully by *Whitby et al.* [1991]; therefore only a brief summary of the method is given here.

Given a lognormal distribution defined as

$$n(\ln D) = \frac{N}{(2\pi)^{1/2} \ln \sigma_g} \exp\left[-0.5\left(\frac{\ln (D/D_g)}{\ln \sigma_g}\right)^2\right] \tag{2}$$

where N is the particle number concentration, D is the particle diameter, and D_g and σ_g the geometric mean diameter and standard deviation of the distribution, respectively, the kth moment of the distribution is defined as

$$M_k = \int_{-\infty}^{\infty} D^k n(\ln D)\, d(\ln D) \tag{3}$$

with the result

$$M_k = N D_g^k \exp\left[\frac{k^2}{2} \ln^2 \sigma_g\right] \tag{4}$$

M_0 is the total number of aerosol particles within the mode suspended in a unit volume of ambient fluid (air). For $k = 2$ the moment is proportional to the total particulate surface area within the mode per unit volume of air. For $k = 3$ the moment is proportional to the total particulate volume within the mode per unit volume of air. The constant of proportionality between M_2 and surface area is π; the constant of proportionality between M_3 and volume is $\pi/6$. Note that the geometric standard deviation is the same no matter which moment is selected. Prediction of three moments of the distribution function will allow both the geometric mean diameter D_g and geometric standard deviation σ_g to be diagnosed as functions of time [*Whitby et al.*, 1991]. Letting the nuclei and accumulation modes be represented by subscripts i and j, respectively, the rate equations for the kth aerosol moment for these two modes are given by

$$\frac{\partial M_{ki}}{\partial t} = -\nabla \cdot (\mathbf{V} M_{ki}) - \frac{\partial}{\partial \sigma}(\dot{\sigma} M_{ki}) + \left(\frac{\partial M_{ki}}{\partial t}\right)_{\text{Diff}} + G_{ki} + C_{kii} + C_{kij} + E_{ki} \tag{5a}$$

$$\frac{\partial M_{kj}}{\partial t} = -\nabla \cdot (\mathbf{V} M_{kj}) - \frac{\partial}{\partial \sigma}(\dot{\sigma} M_{kj}) + \left(\frac{\partial M_{kj}}{\partial t}\right)_{\text{Diff}} + G_{kj} + C_{kjj} + C_{kji} + E_{kj} \tag{5b}$$

Although the choice of the value for the index k is arbitrary and can include noninteger values, for reasons of mathematical simplicity the current version of the model has time-dependent equations for the zeroth, third, and sixth moments of the distribution functions for each size mode. Thus (5a) and (5b) each represents three equations corresponding to values of k equal to 0, 3, and 6. The form of these equations is similar to the species conservation equation, (1). That is, the first three terms on the right side of (5a) and (5b) represent transport of the kth aerosol moment by the horizontal wind, the vertical wind, and turbulent diffusion, respectively. The same comments apply about the use of K theory and the ACM here as for (1). Only the aerosol number moment, corresponding to $k = 0$, is transported for both modes. The aerosol volume moment, which is proportional to the third moment ($k = 3$), is constructed from the mass concentration of the particle constituents (SO_4^{2-}, NH_4^+, and liquid H_2O) by dividing by the appro-

priate densities. SO_4^{2-} and NH_4^+ are transported, while liquid H_2O is equilibrated locally. The last four terms represent, from left to right, the change in aerosol moment by condensational growth, coagulation of particles within the mode, coagulation of particles between the modes, and source emission of particles. Dry deposition of aerosol particles is taken into account as a lower boundary condition in the finite-difference form of the turbulent diffusion term. We discuss the dry deposition algorithm in section 2.6 and describe the details in the appendix. The prediction cycle is also described in the appendix.

2.3. Coagulation

Aerosol size distributions can be altered by particle collision and coagulation. In general, the mathematical representation of coagulation presents formidable difficulties. If, however, only coagulation by Brownian motion is considered, the problem simplifies somewhat [*Friedlander*, 1977; *Seinfeld*, 1986]. If the particle distribution remains lognormal, the problem simplifies further [*Whitby et al.*, 1991]. As described in the Appendix, the integrals representing Brownian coagulation of particles within each mode and between the modes are represented as harmonic means of the coagulation coefficients in the free-molecular and near-continuum particle size regimes. Analytical expressions for these two regimes are given by *Whitby et al.* [1991]. Without serious loss of accuracy, this harmonic mean approach using analytical expressions allows much more efficient calculation of the coagulation terms than would be possible using, for example, numerical quadrature as done by *Giorgi* [1986]. Thus the two intermodal terms for coagulation between particles from modes i and j are given by

$$C_{kij} = \frac{\hat{C}^{fm}_{kij}\hat{C}^{nc}_{kij}}{\hat{C}^{fm}_{kij} + \hat{C}^{nc}_{kij}} \tag{6a}$$

$$C_{kji} = \frac{\hat{C}^{fm}_{kji}\hat{C}^{nc}_{kji}}{\hat{C}^{fm}_{kji} + \hat{C}^{nc}_{kji}} \tag{6b}$$

Intramodal coagulation between particles within mode l, where l denotes either mode i or mode j, is given by

$$C_{kll} = \frac{\hat{C}^{fm}_{kll}\hat{C}^{nc}_{kll}}{\hat{C}^{fm}_{kll} + \hat{C}^{nc}_{kll}} \tag{6c}$$

These expressions are derived and discussed in the appendix.

2.4. Nucleation and Growth

Nucleation, or new particle formation, and growth of existing particles by condensation of vapor are the two pathways for increasing the total aerosol mass. *Middleton and Kiang* [1978] showed that either nucleation or condensation can be the principal pathway depending upon atmospheric conditions such as temperature, relative humidity, the total aerosol surface area, the impingement rate of vapor molecules on the particles, and the chemical production rate of condensable material. For tropospheric sulfate aerosols, binary homogeneous nucleation of sulfuric acid and water vapor appears to be the primary nucleation mechanism. *Easter and Peters* [1993, 1994] have analyzed this process in the context of the marine boundary layer and show that rapid fluctuations in the temperature and relative humidity can lead to bursts of particle production by binary nucleation, especially near the top of the convective mixing layer. *Wexler et al.* [1994] have fit an empirical expression to nucleation rates given by *Jaecker-Voirol* and *Mirabel* [1989] for the critical concentration of sulfuric acid vapor required for the production of 1 particle cm^{-3}. *Kerminen and Wexler* [1994] have derived a simple algorithm for nucleation from an extension of the work of *Middleton and Kiang* [1978]. Our implementation of this algorithm is shown in the appendix. Because simple, accurate parameterizations for particle production processes in point source plumes are not yet available in a form suitable for the regional scale, only a crude representation of new particles resulting from the primary emissions of sulfate is included in this first-generation model; this representation is described in section 2.5.

Aerosol growth by condensation occurs in two steps: the production of condensable material by chemical reaction, and the condensation and evaporation of ambient volatile species on aerosol particles. The production of condensable sulfate resulting in stable particles with increasing sizes is represented explicitly in the RPM. The inclusion of secondary organic and nitrate species will be treated in a subsequent contribution. The growth rates for stable aerosol particles due to vapor condensation are derived in the appendix and are given by

$$G_{ki} = \dot{M}_3\Omega_i\left(\frac{k}{3}\right)\frac{\hat{I}_{ki}}{\hat{I}_{3i}} \tag{7a}$$

$$G_{kj} = \dot{M}_3\Omega_j\left(\frac{k}{3}\right)\frac{\hat{I}_{kj}}{\hat{I}_{3j}} \tag{7b}$$

$\dot{M}_3$ is the rate of increase of M_3 due to condensation and is given by

$$\dot{M}_3 = (6/\pi)(\dot{C}_l/\rho_l) \tag{8}$$

where $\dot{C}_l$ is the chemical production rate of species l and r_l is its density. Note that the growth rate for M_0 is zero; that is, the number of particles does not change with the addition of condensing mass. The other terms are discussed more fully in the appendix.

Water is the most important volatile species condensing upon and evaporating from atmospheric aerosols. The swelling and shrinking of particles with changes in relative humidity is a well-established phenomenon and is discussed fully by *Hänel* [1976] and *Pruppacher and Klett* [1978]. *Pilinis et al.* [1989] show that this swelling and shrinking of particles is an equilibrium process. In view of this, the adjustment of M_3 to relative humidity is modeled as an equilibrium calculation using the increase or decrease of liquid water content specified by the aerosol equilibrium chemistry module discussed above, recognizing that M_0 is not affected by this change in particle size. Because the amount of water present on an aerosol particle at a given relative humidity is directly proportional to the mass of hydrophilic material present, the condensation and evaporation of water may be considered a mass- or volume-based growth process. For such a process, the geometric standard deviation σ_g can easily be shown to be constant. *Tang and Munkelwitz* [1977] show that a nearly monodisperse dry aerosol remains nearly monodisperse (within experimental limitations) during humidification to very high values of relative humidity, giving rather strong experimental evidence that the geometric standard deviation is unaffected by the swelling of particles in response to increasing relative humidity. Thus our equilibrium adjustment to relative humidity holds the geometric standard deviation constant and diagnoses M_6 accordingly.

2.5. Emissions

At present there are inadequate data on the size distribution of aerosols emitted by sources. *McElroy et al.* [1982] have

shown that coal burning yields aerosol emissions in the size range of the nuclei mode. *Whitby* [1978] gives values for D_g and σ_g for a large power plant plume and several near-source situations. In a regional model, emissions are assumed to be mixed instantaneously into the grid cell volume; therefore Whitby's near-source values are relevant. The rate of change of aerosol volume concentration due to source emissions can be determined from the aerosol species mass emissions rate E_l by dividing it by the species density ρ_l. For the work reported here, E_l is the emissions rate for sulfate (taken as H_2SO_4). The rate of change of M_3 due to emissions is

$$\dot{M}_3 = (6/\pi)(E_l/\rho_l) \tag{9}$$

The emissions rate for aerosol number is given by

$$\dot{N} = \frac{\dot{M}_3}{D_g^3 \exp\left((9/2)\ln^2 \sigma_g\right)} \tag{10}$$

and that for any k moment is given by

$$\dot{M}_k = \dot{N} D_g^k \exp\left(\frac{k^2}{2}\ln^2 \sigma_g\right) \tag{11}$$

We then assume

$$E_{ki} = 0.15\dot{M}_k \qquad E_{kj} = 0.85\dot{M}_k \tag{12}$$

The fractional split of the emissions between the modes is a crude representation of the growth of particles occurring in plumes which are not yet represented explicitly in the model. The values chosen for the sizes (D_g and σ_g values of 0.01 μm and 1.6 for the nuclei mode and 0.07 and 2.0 for the accumulation mode, respectively) correspond to the *Whitby* [1978] values for local sources and background, as do the fractional aerosol volumes in the nuclei and accumulation modes (0.17 and 0.83), respectively. This issue will be revisited when plumes are represented explicitly in the model.

2.6. Dry Deposition

We use a conventional deposition velocity approach for dry deposition; however, we apply it to the deposition of the zeroth and third moments of the ith and jth modes using the following equation:

$$v_{dk} = \frac{M_{ki}\hat{v}_{dki} + M_{kj}\hat{v}_{dkj}}{M_{ki} + M_{kj}} \qquad k = 0, 3 \tag{13}$$

where we have assumed uniform particle density in the case of the third moment. The details of our approach are given in the appendix.

3. Model Realization

To build a model as complex as the RPM within a reasonable time frame, a two-path strategy was chosen. First, aerosol chemistry as represented by the MARS module was added to the RADM to investigate the model performance and sensitivity to ammonia uncertainties [*Binkowski and Alapaty*, 1991]. In a parallel effort, we incorporated the Modal Aerosol Dynamics approach of *Whitby et al.* [1991] into the Tagged Species Engineering Model (TSEM) [*McHenry et al.*, 1991]. This allowed us to develop the methods for dealing with volatile components, represented in this case by water, and to investigate the behavior of aerosol size distributions with realistically varying humidity fields, as well as hypothetical reductions in sulfur emissions [*Binkowski and Shankar*, 1992a, b, c]. Results from this path are presented in section 4. The final stage of development is the merging of the two paths into a final model that has sulfate, nitrate, and organic aerosols along with the size distributions and aerosol dynamics. This will be reported in future contributions.

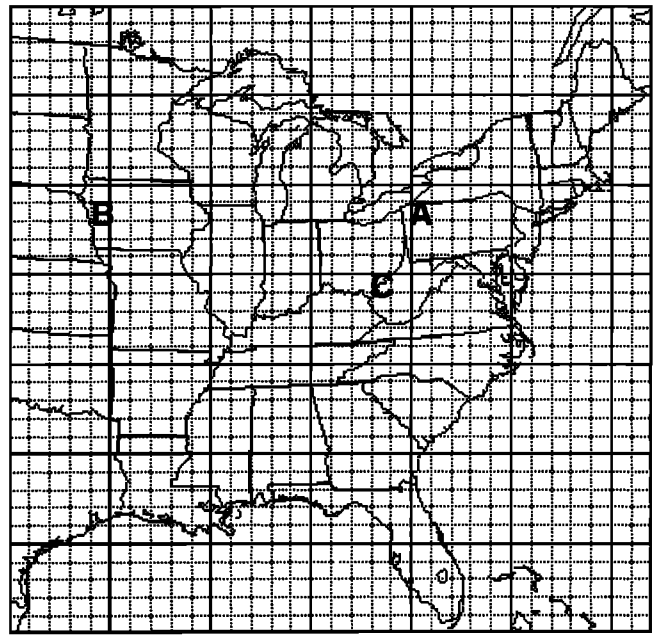

Figure 1. Modeling domain. Selected grid cells are cell A (nominal downwind of source), cell B (rural), and cell C (near source).

4. Preliminary Results From Two Model Simulations

We will describe the results of two model simulations over the RADM domain shown in Figure 1 for a case, denoted as the base case, using the 1985 emissions used for the National Acid Precipitation Assessment Program and for a second case, denoted as b0, which is identical in all respects, except that the ammonia concentrations are set to zero. These two simulation cases model the role of ammonia in neutralizing the sulfate aerosol. For the two simulations the aerosol is either a sulfuric acid solution droplet (b0) or a partly to completely neutralized sulfate solution droplet (base), depending upon the molar ratio of NH_4^+ to SO_4^{2-}. The simulations are for an atmosphere in which clouds are ignored except for attenuating solar radiation. Further, no species of particles other than sulfate aerosols are considered.

We present the results as time histories for the lowest of the 15 model layers in three grid cells shown as A, B, and C in Figure 1. This layer is about 80 m deep. Cell C represents near-source conditions, cell B represents rural conditions, and cell A represents nominal downwind conditions. Other than trying to represent a wide range of emissions (i.e., rural to urban-industrial), the choice of cells A, B, and C was arbitrary. Figure 2a displays the emission rates of sulfur (SO_2 and SO_4^{2-}, taken as H_2SO_4); Figure 2b shows NH_3. Both sets of emission rates (in kilograms per hectare per day) are for a typical summer weekday and are plotted from data given by *Chang et al.* [1990]. These plots show that most of the large sulfur sources

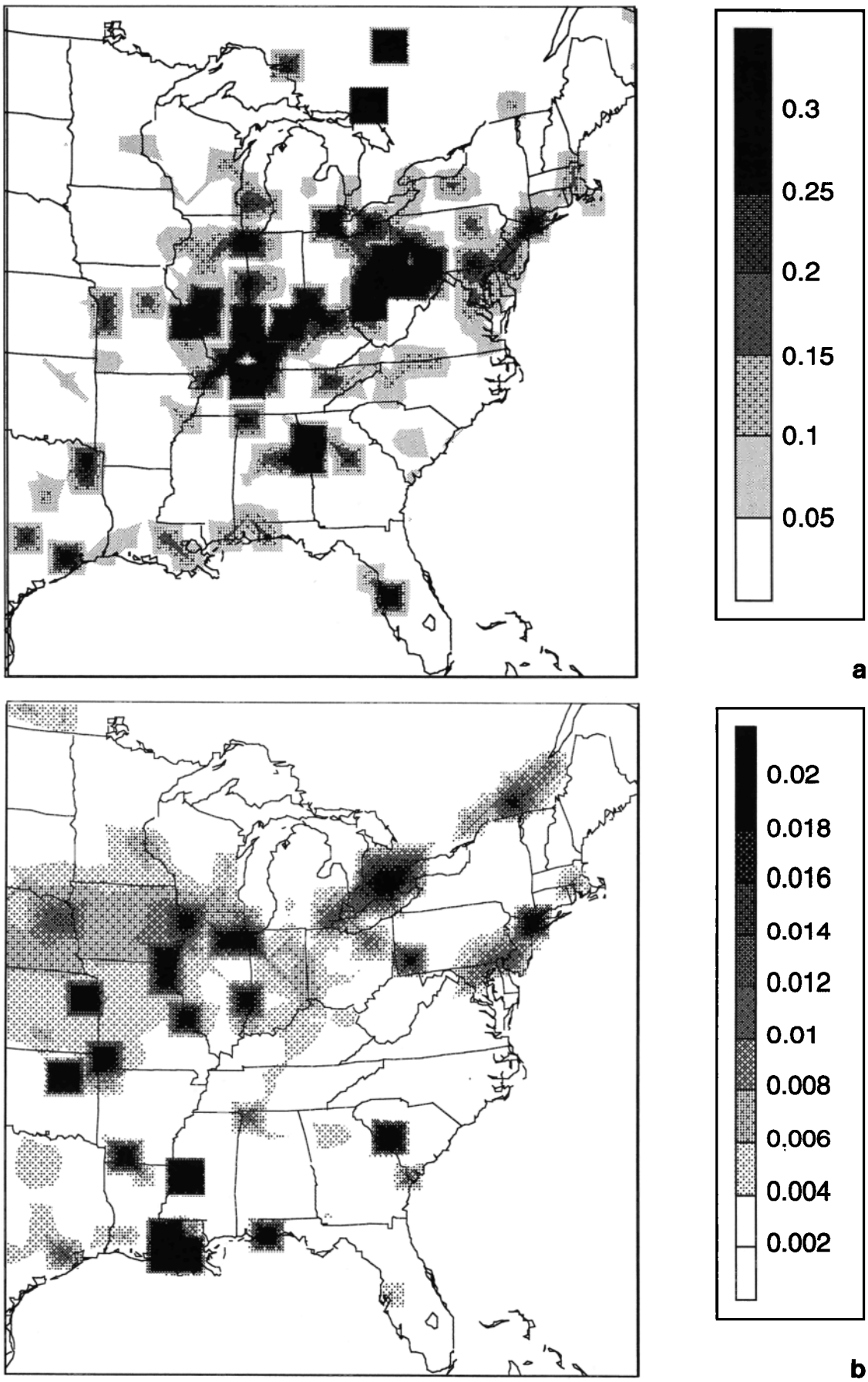

Figure 2. Daily total (a) sulfur (SO_2 + SO_4) and (b) ammonia emissions (kilograms per hectare per day for a summer weekday (1985 NAPAP data from *Chang et al.* [1990]).

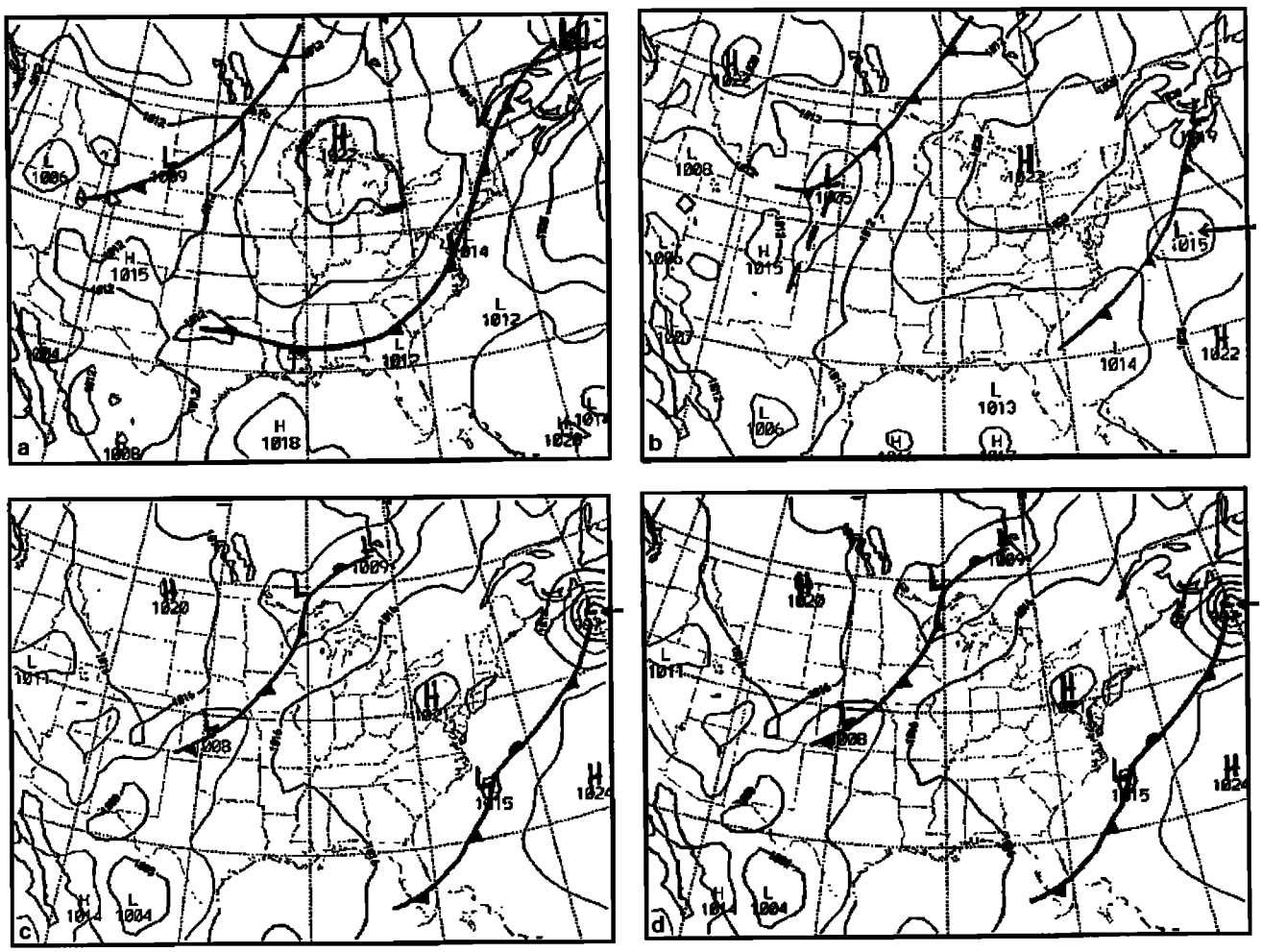

Figure 3. Weather maps for (a) 0000 UT, July 17, 1985, hour 00 of the simulation; (b) 0000 UT, July 18, 1985, hour 24 of the simulation; (c) 0000 UT, July 19, 1985, hour 48 of the simulation; and 0000 UT, July 20, 1985, hour 72 of the simulation.

are east of the main ammonia sources. This implies that ammonia must be transported to the sulfur sources if the sulfates (both emitted and chemically produced) are to be neutralized. This point is addressed further below.

Placet et al. [1990] describe the NAPAP 1985 emissions inventory. The anthropogenic emissions are time-dependent, and the rates are based upon engineering estimates of operating cycles. Natural or biogenic emissions are modulated by atmospheric conditions. Details of how the NAPAP emissions are incorporated into RADM are given by *Chang et al.* [1990]. The RPM follows the RADM usage except as already noted.

The boundary and initial conditions for chemical species concentrations are the same as those used in the RADM and TSEM simulations. Thus the simulation period presented here consists of the last 72 hours of a 120-hour simulation. This limits the influence of both meteorological "spin-up" and chemical equilibration effects on the period under study. For initial and boundary conditions on the aerosol size distributions, the initial sulfate concentration is divided by an average density of 1.8 g cm^{-3} to obtain a volume concentration. Using values from *Whitby* [1978], we split the sulfate volume concentration between modes i and j by a fixed fraction of 0.01 and 0.99, respectively. We then use initial values of D_g and σ_g, respectively, of 0.01 μm and 1.7 for mode i and 0.07 μm and 2.0 for mode j (given by *Whitby* [1978] for the number distributions) to calculate the other moments. These values are used to calculate the aerosol number and sixth-moment concentration emissions rates from the sulfate mass emission rates.

We chose a typical summertime meteorological case from the ensemble of cases developed for the NAPAP work [*Binkowski et al.*, 1990]. The 72-hour simulation began at 0000 UT on July 17, 1985 (Figure 3a) and ended at 0000 UT on July 20 (Figure 3d). This period was relatively dry and dominated by a high-pressure system passing through the model domain. Between hours 36 and 48 of the simulation period (Figures 3b and 3c), a cold front passed through cell B, and rain fell from about hour 40 onward. The winds at cell B were southeasterly and then southerly prior to the frontal passage, after which they became northerly. The winds at cells A and C were northeasterly until the center of the high passed to the east by hour 36. Rain fell in cell C from about hour 63 onward. There was no rain in cell A during the entire simulation period. Figure 4 shows time series plots of grid cell average relative humidity in each of the three grid cells. These humidities are consistent with the weather maps in Figure 3. Note that the highest humidity is in cell B after the rain started. These meteorological inputs for the RPM were provided by a mesoscale numerical weather prediction model (MM4) using four-dimensional

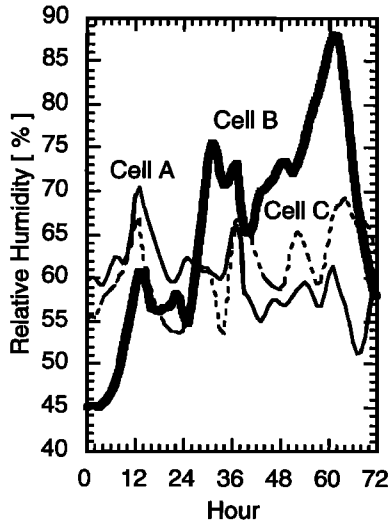

Figure 4. Relative humidities for cells A, B, and C.

data assimilation [*Stauffer and Seaman*, 1990; *Stauffer et al.*, 1991].

As expected from the discussion of Figure 2, the emissions rates shown in Figure 5 for SO_2 (SO2E) and SO_4^{2-} (SO4E) are highest in cell C and lowest in cell B, with the emission rates in cell A having intermediate values. The production rates in cell A increase over the simulation period; those in cell B decrease. The cloudiness and rain occurring after hour 40 diminished the gas phase chemical production of SO_4^{2-}. This same effect is seen in cell C after hour 63. Note that the results presented here do not include the effects of any cloud or aqueous processes other than the inhibition of gas phase production of hydroxyl radicals to oxidize the SO_2. Even with this diminution, the chemical production rate of SO_4^{2-} is much larger than the emission rate for SO_4^{2-}. Note that in cell B the chemical production of SO_4^{2-} exceeds the emission rate of SO_2 between hours 12 and 24. The transients in the emission rates occurring in the morning and evening are caused by the interaction of plume rise with the depth of surface-based turbulent mixing [*Byun and Binkowski*, 1991].

We now discuss the results for chemical concentrations and related information. Figure 6 shows the temporal variations of the SO_4^{2-} and SO_2 concentrations. There are no differences between these concentrations for the base and b0 cases. For the first 36 hours, the sulfate concentrations in cells A and B are comparable and less than 10 $\mu g\ m^{-3}$. After the southerly to southwesterly flow begins at cell A between 36 and 72 hours, the SO_4^{2-} concentration increases to 13 $\mu g\ m^{-3}$, which is less than half that in cell C (36 $\mu g\ m^{-3}$), a very high emission area. The SO_2 concentration increases and peaks at a value of 35 $\mu g\ m^{-3}$ at hour 60. The sulfate in cell A increases partly because of transport from the major source region to the southwest and partly because of the increased production shown in Figure 5. This view is supported by the increase in SO_2 between hours 48 and 60, which corresponds to a minimum in local emissions (Figure 5). The peak at hour 60 is due to the morning peak in emissions. During this same time interval the sulfate concentrations in cell B decrease due to the postfrontal northerly wind transporting cleaner air. This is seen also in Figure 5, where the production rate of sulfate decreases during this time. Although the meteorological information indicated rain, wet deposition is not active in the present simulations.

During the first 12 hours of the simulation, the concentrations of sulfate decrease in all three cells. This is unlikely to be an equilibration problem, because the initialization procedures developed as part of the NAPAP effort mitigate this effect. It appears to be a result of the passage of an essentially clean air mass across the region. The sharp decrease in sulfate concentration in cell C between hours 36 and 48 is associated with the sharp increase in dry deposition shown in Figure 7. There is also a sharp increase in sulfur dioxide concentrations at the same time. The behavior is repeated, although less strongly, just after hour 60. In cell A after hour 60, dry deposition increases, while production (Figure 5) decreases; yet the concentration continues to increase. This is consistent with the interpretation that part of the increase in concentration of sulfate is due to transport.

Ammonium to sulfate molar ratios for the base case (Figure 8) show a strong diurnal variation in all three cells, with nighttime maxima. The large transient in this ratio for all three cells during the first 12 hours is due to the decrease of sulfate

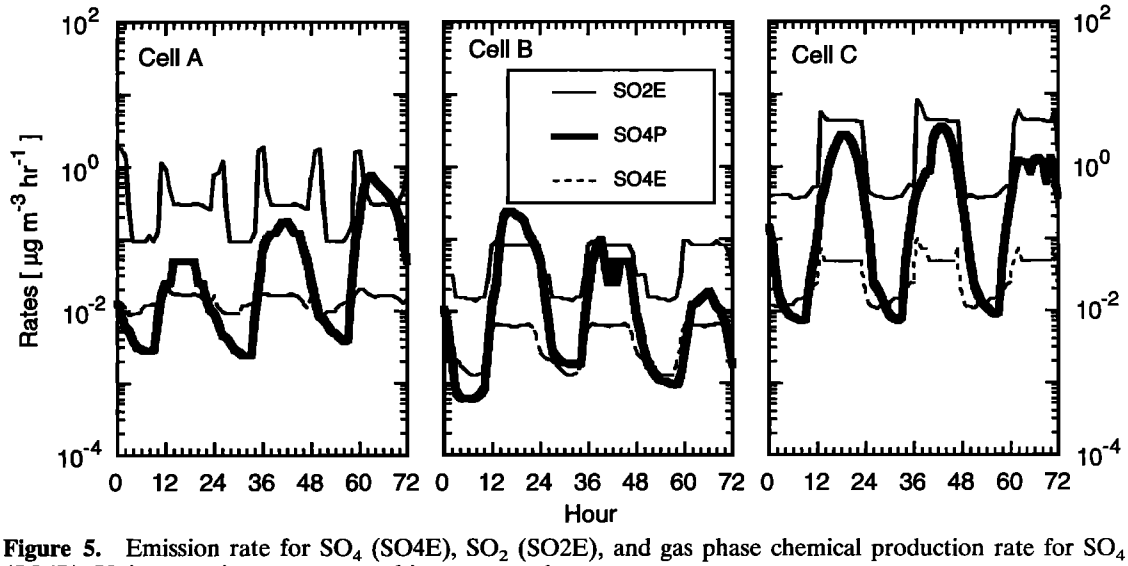

Figure 5. Emission rate for SO_4 (SO4E), SO_2 (SO2E), and gas phase chemical production rate for SO_4 (SO4P). Units are micrograms per cubic meter per hour.

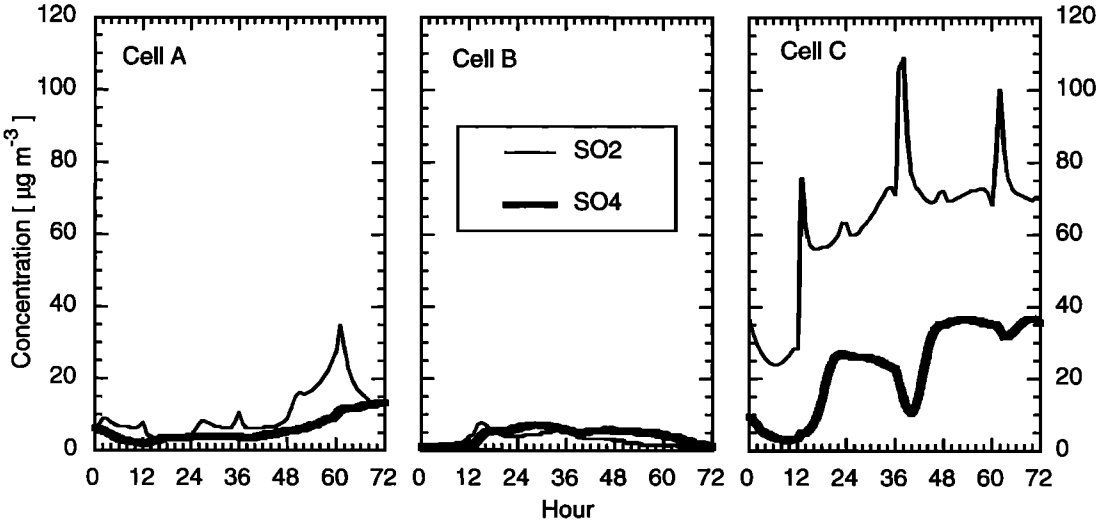

Figure 6. Sulfate (SO_4) and sulfur dioxide (SO_2) concentrations (micrograms per cubic meter). Both base and b0 cases are the same.

concentrations from the initial conditions. Our interpretation is based upon the understanding that ammonia is emitted from the surface and transported vertically by turbulent eddies. At night these eddies are usually weak, and ammonia concentrations can increase at lower altitudes (say, in the lowest grid cell). With the initiation of daytime thermal convection, ammonia is distributed over a deeper layer, with a consequent decrease in concentration. Sulfate concentrations do not show such a pronounced diurnal variation because sulfate is a secondary species (i.e., the formation of sulfate is mainly due to the oxidation of sulfur dioxide, which dominates over the direct emission of sulfate, as seen in Figure 5). The molar ratios are largest in cell B, which is in the heart of the ammonia source region (Figure 2b). The molar ratio in cell C is the smallest because of the large sulfur sources and small ammonia sources. The values in cell A are intermediate and, in addition to the strong diurnal behavior, display a trend inverse to the sulfate concentrations shown in Figure 6. Note that a molar ratio of 2:1 indicates fully neutralized sulfate (ammonium sulfate) and is present during the first 12 and last 3 hours in cell B.

The particle water mass fraction (Figure 9) results from an equilibrium between the aerosol particles and relative humidity [*Pilinis et al.*, 1989]. The amount of water present is determined by the ammonium to sulfate ratio. Thus the water mass fraction is quite different for the base and b0 cases. Cell B shows the most striking difference. The curve for the base case is seen to be strongly (inversely) related to the molar ratio plot for cell B in Figure 8. Cell C shows little or no difference between the base and b0 cases after hour 24. This is related to the very small values of the molar ratio in Figure 8. The initial transient in molar ratio in Figure 8 for all three cells is reflected in the minimum values in water mass fraction. These differences in water mass fraction are associated with differences in average particle density (Figure 10). Minima in water mass fraction are associated with maxima in average particle density. Note that there is also a difference in average particle

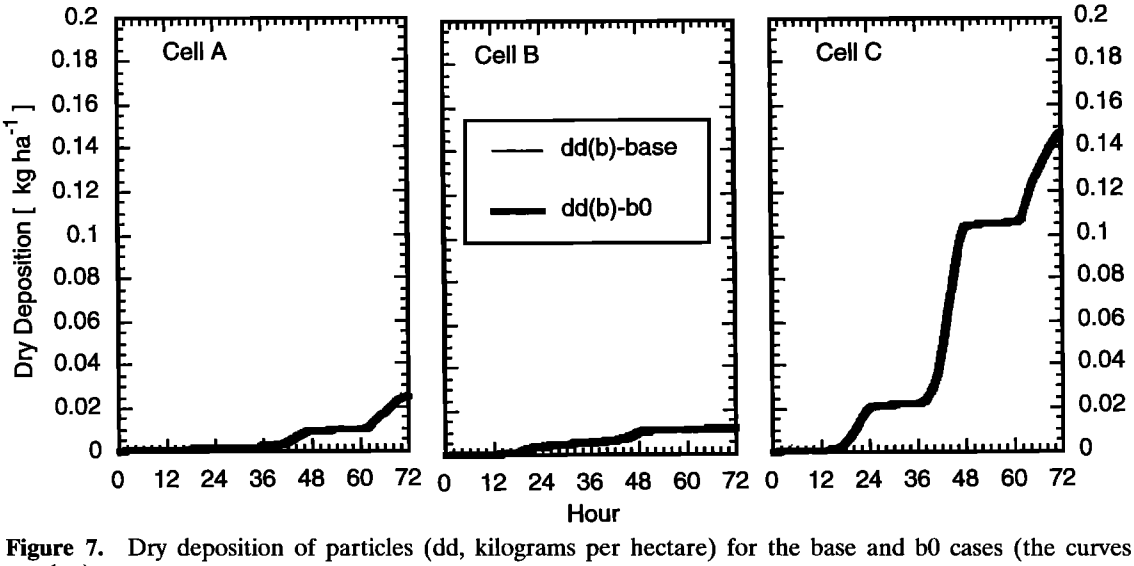

Figure 7. Dry deposition of particles (dd, kilograms per hectare) for the base and b0 cases (the curves overlap).

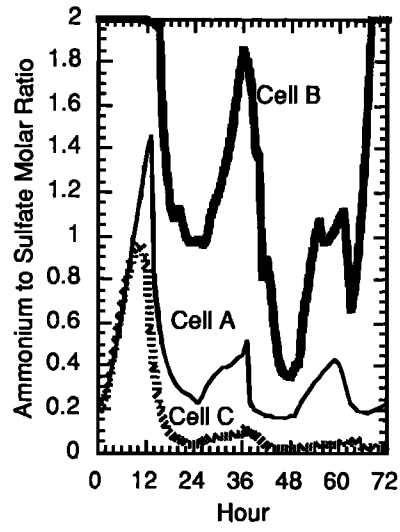

Figure 8. Ammonium to sulfate molar ratios for cells A, B, and C for the base case. This ratio is uniformly zero for the b0 case.

refractive index associated with water mass fraction, with higher values of water mass fraction being associated with smaller refractive indices; that is, the curves of average refractive index should behave like the curves for average particle density. This means that the level of neutralization of sulfate has important optical effects [*Binkowski and Shankar*, 1992b].

The total particle mass concentration (Figure 11) is similar to that of sulfate but shows differences between the base and b0 cases. As expected from the discussion thus far, the differences are the largest in cell B and smaller in cells A and C. Model simulations (not shown here) in which nucleation was omitted partitioned the new mass generated by sulfate production between the modes, causing the j mode to grow. In the model results reported here, nucleation is in effect and, as described in the appendix, the new particles are distributed in the i mode. Thus the mass represented by the newly formed particles increases the i mode mass and number (Figure 12).

To better illustrate this shift in mass, we now discuss Figure 13, which shows plots of the steady state concentration C_{ss}, and the critical concentration C_{crit} (both are defined in the appendix) for each of the three grid cells. In cell A, new particles are formed around hour 12 and hour 36. In cells B and C, new particles are formed around hour 12. Regional maps (not shown here) of the occurrence of nucleation (C_{ss} exceeds C_{crit}) indicate that there is a broad geographic region of occurrence in grid cells lying between cells A, B, and C during hours 12 to 20. During hours 36 through 42, a region of nucleation extends east and north of cell C. During hours 60 through 66, the region is again to the east and north of cell C and smaller in extent than on the previous day. It would seem that the production rate of sulfate exceeds the condensation rate for most of the daylight hours on the first 2 days and that these new particles are transported to cells C and A. There must be transport to cell C because there is no nucleation in this cell after hour 48, but the number concentration of i mode particles (Figure 12) increases, and there is strong dry deposition (Figure 8). The number concentrations in Figure 12 are generally within the range of values reported in Table 1 of *Whitby* [1978]. The range for cell C, however, is somewhat larger than Whitby's background and local sources category. This is to be expected, since the omission of clouds and aqueous production of sulfate removes a mechanism for adding mass to the j mode. This in turn reduces the total surface area for condensation of mass produced by gas phase chemistry and shifts the mass produced to the i mode via new particle production.

In Figures 14 (base case) and 15 (b0 case), we see the size distributions of particle mass for six 12-hour averaging periods ending at the hours shown. This was accomplished by constructing the distributions hourly and averaging these distributions over 12-hour time intervals. This procedure mimics the current observational practice of collecting surface-based samples of particle distributions. Comparing Figures 14a and 15a, we see that peak values for the averaged total mass distributions for the period ending at hour 72 in cells A and B are slightly larger in the b0 case than in the base case. Note also that for both the base and b0 cases the distributions become narrower and peak at smaller diameters in cells A and C, while in cell B the distributions broaden with time and retain more of a bimodal character. Figures 14b and 15b show the sulfate

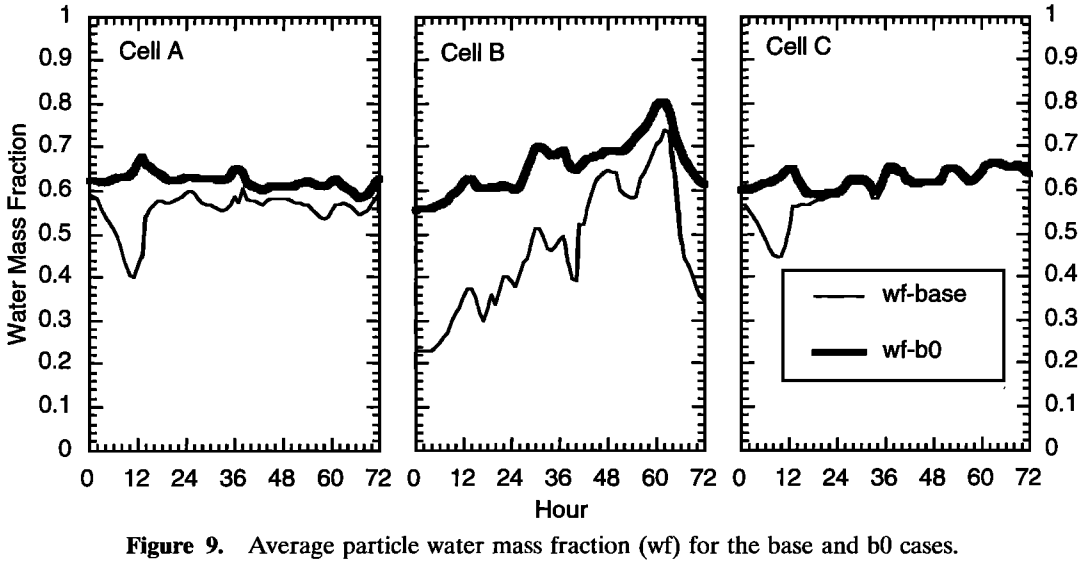

Figure 9. Average particle water mass fraction (wf) for the base and b0 cases.

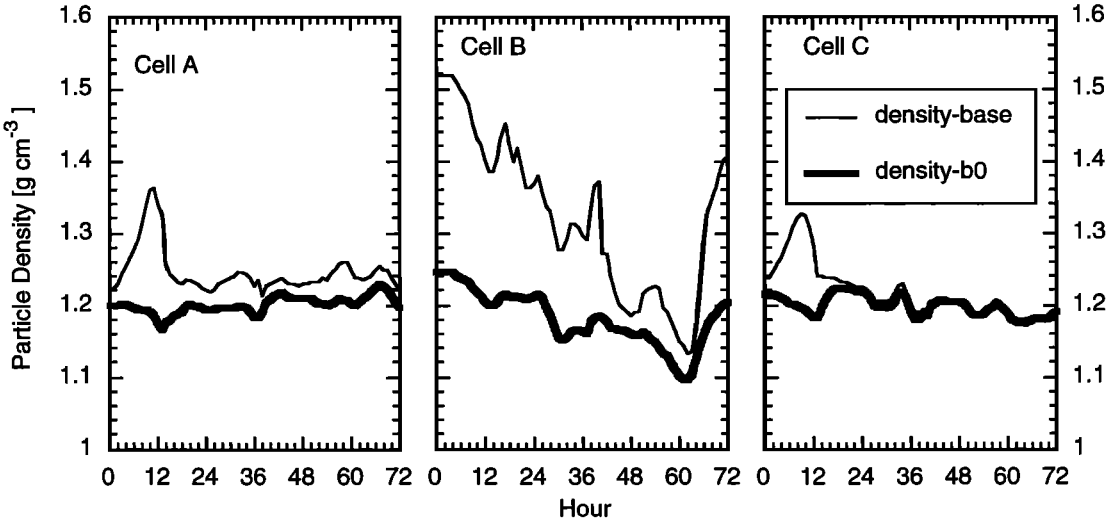

Figure 10. Average particle density (grams per cubic centimeter) for the base and b0 cases.

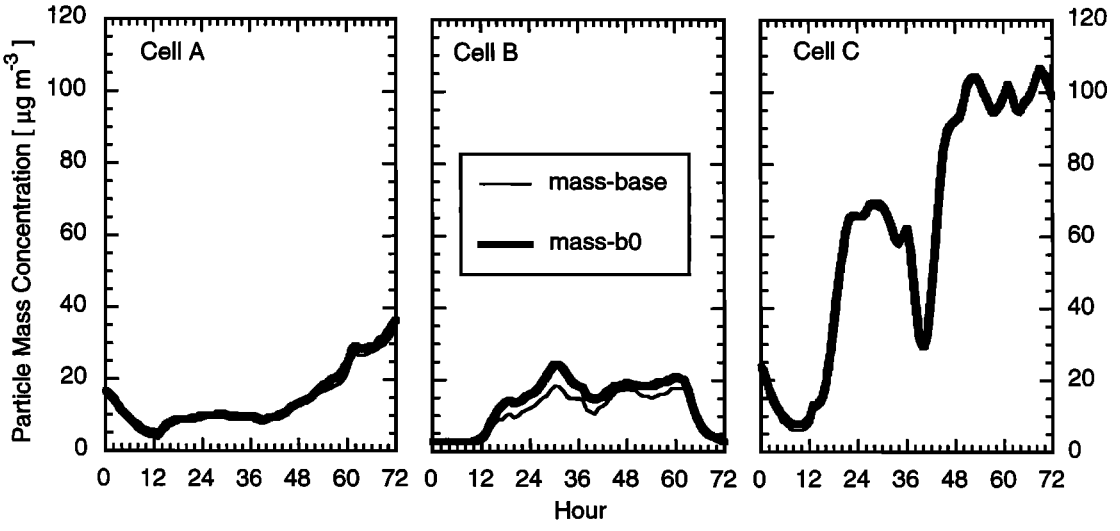

Figure 11. Total particle mass concentration (micrograms per cubic meter) for the base and b0 cases.

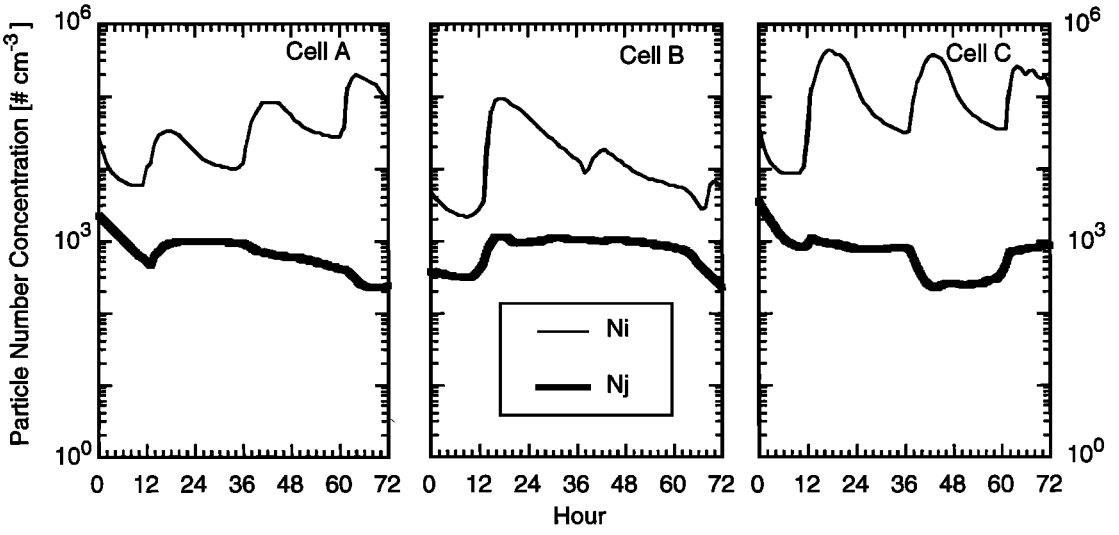

Figure 12. Particle number concentration (number per cubic centimeter) in *i* and *j* modes. Differences between base and b0 cases are indistinguishable in this plot.

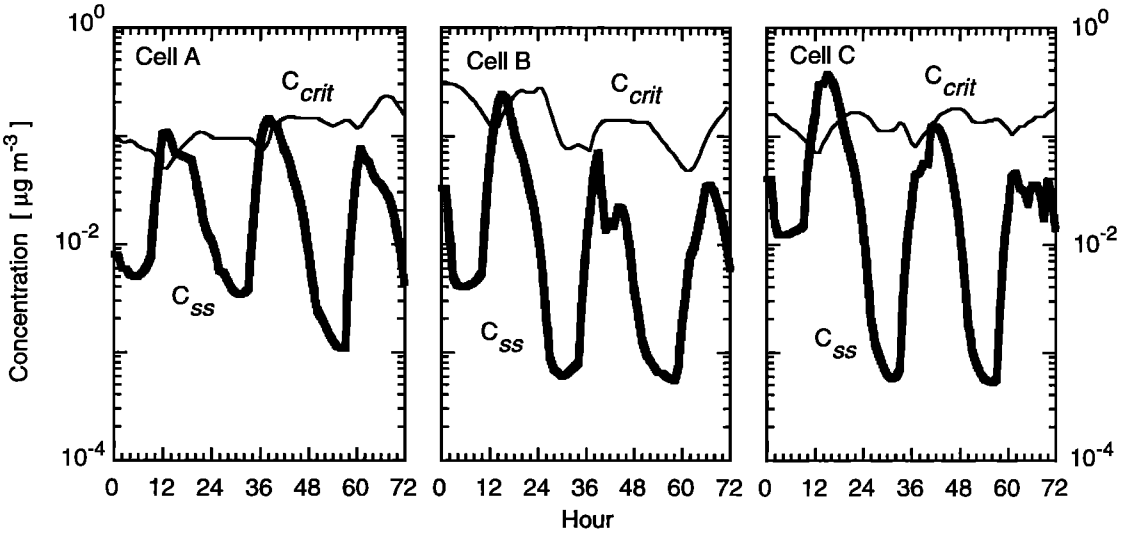

Figure 13. Critical and steady state concentrations (micrograms per cubic meter) for base case. Those for the b0 case are very similar. See the appendix for definitions and details.

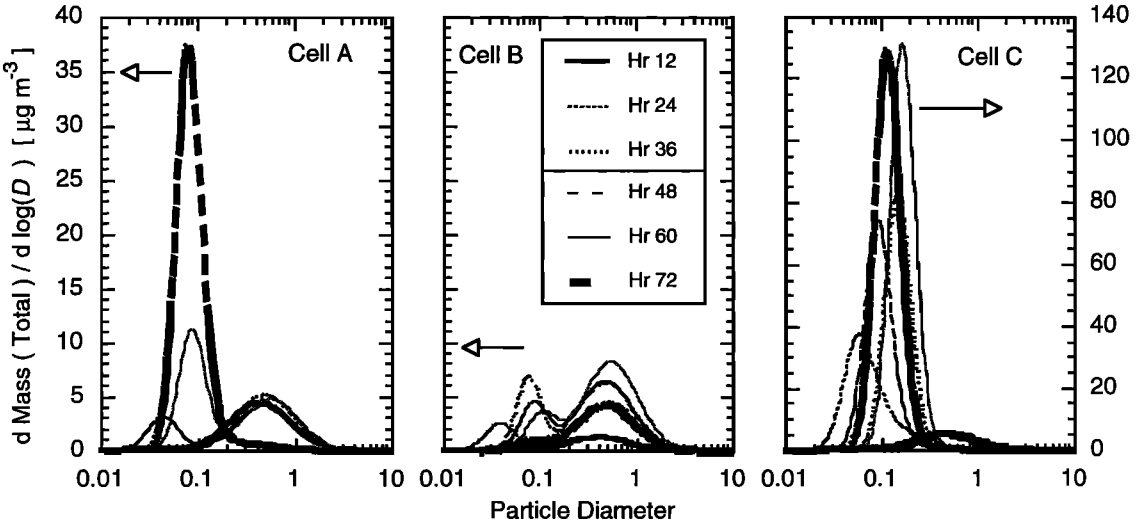

Figure 14a. Total mass size distribution for the base case. Note scale change for cell C. The plots are for 12-hour averages ending at the time shown.

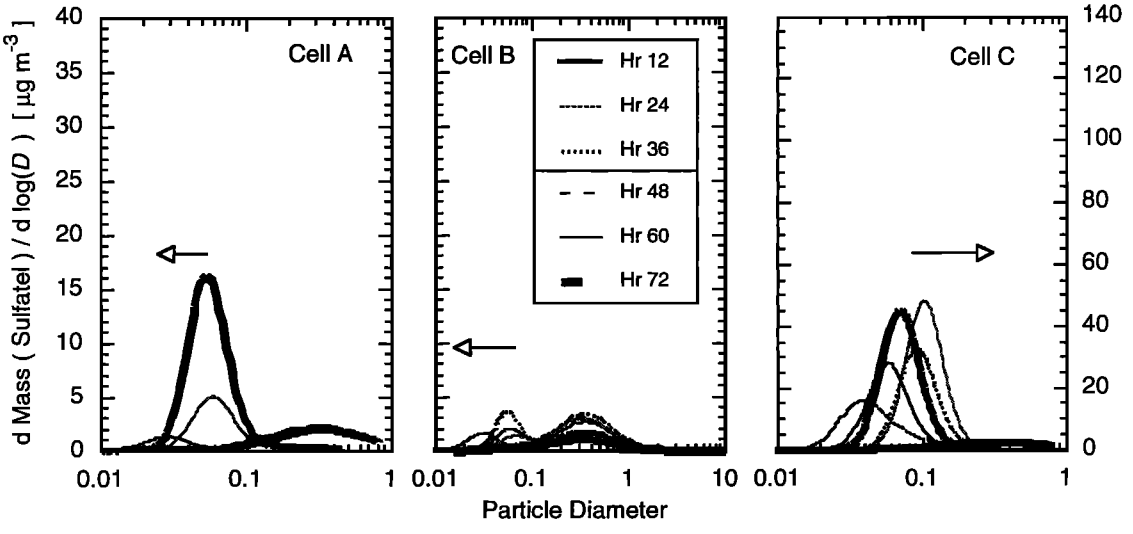

Figure 14b. Sulfate mass size distribution for the base case. Note scale change for cell C. The plots are for 12-hour averages ending at the time shown.

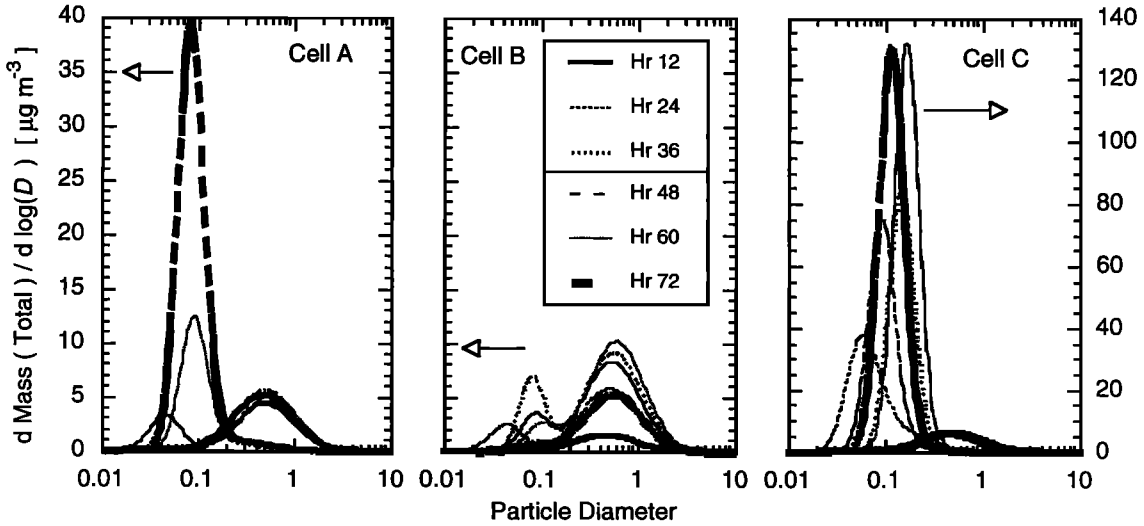

Figure 15a. Total mass size distribution for the b0 case. Note scale change for cell C. The plots are for 12-hour averages ending at the time shown.

mass distribution for the base and b0 cases, respectively. These plots were constructed assuming that water removal does not affect the geometric standard deviations, σ_{gi} and σ_g. Then "dry" diameters can be calculated and the sulfate mass distributions (including ammonium) constructed. Comparing Figures 14b and 15b, we see behavior similar to that for total mass.

The size distributions in Figure 14 and 15 are representative of the rather restrictive experimental conditions described above, that is, that we consider only sulfate aerosol particles. Gas phase oxidation of sulfur dioxide is the sole mechanism for the production of secondary sulfate. Clouds are ignored except for their attenuation of solar radiation. The result of these conditions is that new particle production by nucleation becomes relatively more important and the size distribution shifts to smaller sizes with time. Results of extended work [*Binkowski and Shankar*, 1994; *Shankar and Binkowski*, 1994] not shown here, which includes clouds, confirms this interpretation. This work will be fully reported in a subsequent paper.

5. Summary and Conclusions

We have developed an Eulerian model, the RPM, that provides a potentially important tool for investigating tropospheric aerosol behavior. By using analytic functions for aerosol size distributions in two size ranges of particles, we have provided a computationally efficient alternative to the sectional approach on a regional scale. Incorporating the most important aerosol processes into the RADM allows us to build a multipurpose modeling system that has most of the relevant chemistry and physics of trace gases and aerosols necessary for mesoscale lower tropospheric studies. The model provides a platform for testing alternative formulations for aerosol processes and their effects on aerosol concentration and deposition. Model refinements discussed in the next section will enhance the applicability of the model to such environmental problems as the fate of semivolatile organic compounds in the atmosphere, the response of aerosols to hypothetical control

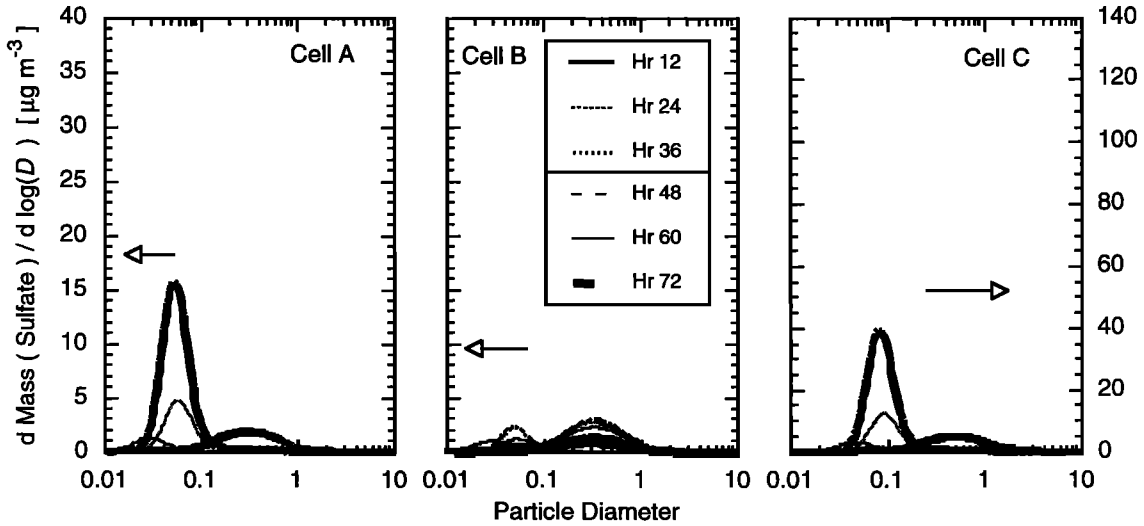

Figure 15b. Sulfate mass size distribution for the b0 case. Note scale change for cell C. The plots are for 12-hour averages ending at the time shown.

strategies [*Binkowski and Shankar*, 1992a, c], or the study of the optical and radiative behavior of atmospheric aerosols [*Binkowski and Shankar*, 1992b].

This preliminary study shows that the neutralizing characteristic of ammonia strongly influences the aerosol LWC, and therefore the total aerosol volume concentration, because a molar ratio of NH_4^+-to-SO_4^{2-} greater than 1.0 results in a lower LWC at the same relative humidity. The results for volume concentration show that the strongest influence is in the rural region, the next strongest in the downwind-of-source region, and the weakest in the near-source region. Because acidic particles pose a potential health hazard, neutralization is an issue for human health as well. The importance of neutralization leads immediately to the corollary that better ammonia emissions inventories are needed, along with a better understanding and formulation of the process of neutralization.

6. Future Work

As mentioned in section 2.1, future versions of the RPM will include secondary nitrate and organic species as well as primary emissions of elemental carbon. Secondary organic aerosols will be modeled at first, following a suggestion of *Grosjean and Seinfeld* [1989]. They have proposed that the condensable material resulting from chemical reactions of organic species may be represented by assigning a fraction of the emission rate of a given species to be a production rate for secondary organic aerosols. This is the first approach to be taken in the RPM. *Pandis et al.* [1992] have developed an improved method for forming secondary organic aerosols that gives explicit yields; this method will be incorporated into subsequent versions of RPM. Consideration of these additional species, as well as the treatment of cases with very low relative humidity, and the presence of the precipitating solid phase require a much more complete treatment of aerosol thermodynamics and chemistry. *Clegg et al.* [1992] and *Clegg and Pitzer* [1992] have presented an approach that allows the solubilities of aerosols ranging from aqueous solutions to dry fused salts to be treated as functions of relative humidity. Their approach will be adapted for inclusion in future versions of the RPM. Semivolatile organic compounds, many of which are toxic, can exist in either gaseous or particulate form [*Pankow*, 1987]. We also plan to include provisions for treatment of this type of organic material in the RPM.

The work presented here concentrates on anthropogenic aerosols. Soil-derived and marine materials are also major contributors to atmospheric aerosols. Some important pollution problems are associated with the resuspension of material that has been dry-deposited and adsorbed onto soil particles. As mentioned in the introduction, *Westphal et al.* [1988] presented model results for the mobilization and transport of Saharan dust. Our approach will model the soil-derived and marine aerosols by adding a third mode for these larger particles. Sedimentation effects then must be addressed because of the larger particle sizes. Results of simulations including these improvements will be reported in future contributions.

Interaction of aerosol particles with cloud droplets is another important process that must be included. *Chaumerliac* [1984] and *Chaumerliac et al.* [1986] presented a methodology for this interaction. We have adopted their approach, which uses a two-step process suggested by *Slinn* [1974] in which scavenging by in-cloud mechanisms coagulates aerosol particles with cloud water droplets, and rain removes the material from clouds. We have extended this method to include a simple parameterization of nucleation scavenging as well [*Binkowski and Shankar*, 1994; *Shankar and Binkowski*, 1994]. Results of this work will be reported in part 2 of this paper.

Appendix: Aerosol Dynamics Equations

A1. Coagulation

Coagulation of particles is discussed fully by *Whitby et al.* [1991]. The main points of the discussion are as follows. All coagulation of aerosol particles is in response to Brownian motion. Aerosol volume is conserved during coagulation; the volume of a particle resulting from the coagulation of two other particles is equal to the sum of the volumes of the coagulating particles. Thus the diameter of the resulting particle is taken as the cube root of the sum of the cubes of the diameters of the coagulating particles. In the bimodal approach of the RPM, intramodal coagulation results in a particle within that mode; intermodal coagulation of a particle in the ith mode with one in the jth mode always results in a particle in the jth mode. That is, there is a transfer of mass concentration from the smaller to the larger mode accompanied by a decrease in particle number in the smaller mode, but no increase in particle number occurs in the larger mode. Intramodal coagulation is represented as follows.

$$\hat{C}_{ku} = \frac{1}{2}\int_0^\infty\int (D_1^3 + D_2^3)^{k/3}\beta(D_1, D_2)n_i(D_1)n_i(D_2)\,dD_1\,dD_2 - \int_0^\infty\int D_1^k\beta(D_1, D_2)n_i(D_1)n_i(D_2)\,dD_1\,dD_2 \quad \text{(A1)}$$

$$\hat{C}_{kjj} = \frac{1}{2}\int_0^\infty\int (D_1^3 + D_2^3)^{k/3}\beta(D_1, D_2)n_j(D_1)n_j(D_2)\,dD_1\,dD_2 - \int_0^\infty\int D_1^k\beta(D_1, D_2)n_j(D_1)n_j(D_2)\,dD_1\,dD_2 \quad \text{(A2)}$$

Intermodal coagulation is represented by

$$\hat{C}_{kij} = -\int_0^\infty\int D_1^k\beta(D_1, D_2)n_i(D_1)n_j(D_2)\,dD_1\,dD_2 \quad \text{(A3)}$$

$$\hat{C}_{kji} = \int_0^\infty\int (D_1^3 + D_2^3)^{k/3}\beta(D_1, D_2)n_j(D_1)n_i(D_2)\,dD_1\,dD_2 - \int_0^\infty\int D_1^k\beta(D_1, D_2)n_j(D_1)n_i(D_2)\,dD_1\,dD_2 \quad \text{(A4)}$$

where $\beta(D_1, D_2)$ is the Brownian coagulation kernel [*Friedlander*, 1977; *Seinfeld*, 1986].

Whitby et al. [1991] show how these integrals can be simplified by examining size regimes expressed in terms of the Knudsen number Kn, which is defined as the ratio of the mean free

path of air to the radius of the particle. At standard conditions, the mean free path for air is about 0.065 μm.

Value of Kn	Size Regime
$10 < Kn$	free molecule (fm)
$1 < Kn \leq 10$	transition
$0.1 < \mathrm{Kn} \leq 1$	near continuum (nc)
$Kn \leq 0.1$	continuum

For Knudsen numbers greater than 10 the particles may be thought of as free molecules, and the physical picture of the kinetic theory of gases is relevant. For Knudsen numbers less than 0.1, the particles may be visualized as being suspended in a fluid. For Knudsen numbers between 1 and 10 (the transition regime), various empirical corrections are available to describe the behavior of particles [*Friedlander*, 1977; *Seinfeld*, 1986]. Whitby et al. give complete details on these corrections and show specialized equations developed for the present approach. They also show that the coagulation kernel may be represented by combining two asymptotic forms, the free molecular form β^{fm} and the near continuum form β^{nc}, given by

$$\beta^{\mathrm{fm}} = \left(\frac{3kT}{\rho_{\mathrm{p}}}\right)^{1/2}\left(\frac{1}{D_1^3} + \frac{1}{D_2^3}\right)^{1/2}(D_1 + D_2)^2 \tag{A5}$$

$$\beta^{\mathrm{nc}} = \left(\frac{2kT}{3\mu}\right)(D_1 + D_2)\left[\frac{1}{D_1} + \frac{1}{D_2} + 2.492\lambda\left(\frac{1}{D_1^2} + \frac{1}{D_2^2}\right)\right] \tag{A6}$$

where λ is the mean free path of air (centimeters). The common way of treating coagulation also would include a coagulation kernel appropriate to the transition regime and a numerical quadrature for all three regimes, as done by *Giorgi* [1986], for example. Numerical quadratures are, however, computationally intensive. *Whitby et al.* [1991] follow a different approach. They show that the free-molecular and near-continuum coagulation integrals may be evaluated analytically. For free-molecular coagulation and near-continuum coagulation, the integrals corresponding to (A1) through (A4) are given by $\hat{C}_{kij}^{\mathrm{fm}}$, $\hat{C}_{kbb}^{\mathrm{fm}}$, $\hat{C}_{kij}^{nc}$, $\hat{C}_{kbb}^{nc}$, respectively. The free-molecular form (A5) requires some algebraic manipulation before integration and table lookup for a constant (of the order of 1) relevant to intermodal and intramodal coagulation to achieve this simplification. *Whitby et al.* [1991] then use a device proposed by *Pratsinis* [1988] that expresses the coagulation coefficient in terms of the harmonic mean between only the free-molecular and near-continuum expressions. The two intermodal terms thus are given by (6a) and (6b)

$$C_{kij} = \frac{\hat{C}_{kij}^{\mathrm{fm}}\hat{C}_{kij}^{\mathrm{nc}}}{\hat{C}_{kij}^{\mathrm{fm}} + \hat{C}_{kij}^{\mathrm{nc}}}$$

$$C_{kji} = \frac{\hat{C}_{kji}^{\mathrm{fm}}\hat{C}_{kji}^{\mathrm{nc}}}{\hat{C}_{kji}^{\mathrm{fm}} + \hat{C}_{kji}^{\mathrm{nc}}}$$

while both intramodal terms are of the form (equation (6c))

$$C_{kii} = \frac{\hat{C}_{kii}^{\mathrm{fm}}\hat{C}_{kii}^{\mathrm{nc}}}{\hat{C}_{kii}^{\mathrm{fm}} + \hat{C}_{kii}^{\mathrm{nc}}}$$

Whitby et al. [1991] argue that in general, this method is within 20% of the method that includes the transition regime, and, for typical atmospheric values of σ_{gi} and σ_{gj} of 1.5 or greater [*Whitby*, 1978], the difference is about 10%. *Pratsinis* [1988] also shows that in the transition regime, the difference between the harmonic mean approach and the familiar Fuchs-Sutugin method is of the order of 15%.

A2. Growth

Aerosol particles grow by the addition of new material onto existing particles. Neglecting the Kelvin effect, the growth rates for the kth moment of the ith and jth modes of the aerosol distribution are given by [*Whitby et al.*, 1991]

$$G_{ki} = \frac{2k}{\pi}\Psi_T I_{ki} \tag{A7}$$

$$G_{kj} = \frac{2k}{\pi}\Psi_T I_{kj} \tag{A8}$$

$$I_{ki} = \int_0^\infty D^{k-3}\psi(D)n_i(D)\,dD \tag{A9}$$

$$I_{kj} = \int_0^\infty D^{k-3}\psi(D)n_j(D)\,dD \tag{A10}$$

where Ψ_T is a size-independent component of the growth law given by

$$\Psi_T = \frac{m_w p_s(S_v - 1)}{\rho_l \mathbf{R} T}$$

and $\psi(D)$ is the size-dependent component and has two asymptotic forms for free-molecular and near-continuum size ranges given by

$$\psi^{fm} = \frac{\pi\alpha\bar{c}}{4}D^2 \tag{A11}$$

$$\psi^{nc} = 2\pi D_v D \tag{A12}$$

Integrating (A11) and (A12) and applying the same averaging concept developed for particle coagulation, the integrals (A9) and (A10) are given by

$$I_{ki} \cong \hat{I}_{ki} \equiv \left(\frac{\hat{I}_{ki}^{\mathrm{fm}}\hat{I}_{ki}^{\mathrm{nc}}}{\hat{I}_{ki}^{\mathrm{fm}} + \hat{I}_{ki}^{\mathrm{nc}}}\right) \tag{A13}$$

$$I_{kj} \cong \hat{I}_{kj} \equiv \left(\frac{\hat{I}_{kj}^{\mathrm{fm}}\hat{I}_{kj}^{\mathrm{nc}}}{\hat{I}_{kj}^{\mathrm{fm}} + \hat{I}_{kj}^{\mathrm{nc}}}\right) \tag{A14}$$

$$\hat{I}_{ki}^{\mathrm{fm}} = \frac{\pi\alpha\bar{c}}{4}M_{(k-1)i}$$
$$\hat{I}_{ki}^{\mathrm{nc}} = 2\pi D_v M_{(k-2)i} \tag{A15}$$

$$\hat{I}_{kj}^{\mathrm{fm}} = \frac{\pi\alpha\bar{c}}{4}M_{(k-1)j}$$
$$\hat{I}_{kj}^{\mathrm{nc}} = 2\pi D_v M_{(k-2)j} \tag{A16}$$

Pratsinis [1988] showed that this type of averaging approach for particle growth is a very good approximation for the transition regime. Values for the vapor diffusivity (0.08) and accommodation coefficient (0.05) are taken from *Van Dingenen and Raes* [1991].

If the growth processes are fast compared with the generation of condensable vapor, a steady state develops where the volume growth rate of the particles is equal to the production

rate of the vapor. The total growth rate of particle third moment is the sum of the growth rate of the two modes:

$$G_3 = G_{3i} + G_{3j}$$

This total must then be equal to $\dot{M}_3$, the rate of production of third moment from condensable vapor:

$$G_3 = \dot{M}_3$$

The fraction of the material injected into each mode is given by the coefficients Ω_i and Ω_j:

$$\Omega_i \equiv \left(\frac{G_{3i}}{G_{3i} + G_{3j}}\right) = \left(\frac{\hat{I}_{3i}}{\hat{I}_{3i} + \hat{I}_{3j}}\right) \quad \text{(A17)}$$

$$\Omega_j \equiv \left(\frac{G_{3j}}{G_{3i} + G_{3j}}\right) = \left(\frac{\hat{I}_{3j}}{\hat{I}_{3i} + \hat{I}_{3j}}\right) \quad \text{(A18)}$$

Substituting (A13) and (A14) into (A7) and (A8), recognizing that the fractional growth rates for each mode are the product of (A17) and (A18) with $\dot{M}_3$, and noting that the growth rate for any moment can be expressed in terms of the third-moment growth rate, we then can write the final expressions for the condensational growth terms for any moment as (equations (7a) and (7b)

$$G_{ki} = \dot{M}_3 \Omega_i \left(\frac{k}{3}\right) \frac{\hat{I}_{ki}}{\hat{I}_{3i}}$$

$$G_{kj} = \dot{M}_3 \Omega_j \left(\frac{k}{3}\right) \frac{\hat{I}_{kj}}{\hat{I}_{3j}}$$

Note that Ψ_T has cancelled out in (A17) and (A18) as well as in (7a) and (7b). The rate of increase of M_3 by vapor condensation, $\dot{M}_3$, is obtained from the vapor condensation rate (mass per unit time) as follows. Recall that total aerosol volume concentration is given by

$$V = (\pi/6) M_3 \quad \text{(A19)}$$

Dividing the vapor condensation rate by $(\pi/6)$ times the density of the condensed vapor yields the rate of increase of M_3 due to vapor condensation (equation (8)).

A3. Nucleation

Kerminen and Wexler [1994] (hereinafter referred to as KW) have described a parameterization of nucleation which we have adapted to our modeling paradigm. They start with the rate equation for the production of sulfuric acid concentration C (micrograms per cubic meter)

$$dC/dt = P - C\tau_\infty^{-1} \quad \text{(A20)}$$

where P is the rate of gas phase production of sulfuric acid and the timescale τ_∞ (seconds) for condensation on the existing particles is given by

$$\tau_\infty^{-1} = I_{ki} + I_{kj} \quad \text{(A21)}$$

KW argue that τ_∞ is short enough that both τ_∞ and P can be held constant over some small time interval and the rate equation can be solved as

$$C(t) = C_{ss} - [C_{ss} - C_0] \exp(-t\tau_\infty^{-1}) \quad \text{(A22)}$$

where the steady state concentration is given by

$$C_{ss} = P\tau_\infty \quad \text{(A23)}$$

KW also give an empirical equation which was fit by *Wexler et al.* [1994] to the nucleation rates of *Jaecker-Voirol and Mirabel* [1989] for a critical concentration of sulfuric acid C_{crit} (micrograms per cubic meter) above which new particles are formed,

$$C_{crit} = 0.16 \exp(0.1T - 3.5\text{rh} - 27.7) \quad \text{(A24)}$$

where T (kelvins) is temperature, and rh is fractional relative humidity [0, 1]. Thus when C_{ss} is greater than C_{crit}, new particles are formed from the excess and with the rest of the mass being condensed on the existing particles. As mentioned above, this follows from the ideas set forth by *Middleton and Kiang* [1978]. KW use a sectional paradigm and assign all of the mass of newly formed particles to the smallest size bin. In the modal paradigm, we distribute these newly formed particles in the i mode using the same modal parameters as for initialization and emissions; that is, D_g and σ_g have values of 0.01 μm and 1.6, respectively.

A4. Dry Deposition

Deposition for monodisperse aerosols is governed by two key quantities, the Brownian particle diffusivity

$$D_p = \left(\frac{k_b T}{3\pi\nu\rho_{air} D}\right) Cc \quad \text{(A25)}$$

and the gravitational settling velocity

$$v_G = \left[\frac{g}{18\nu}\left(\frac{\rho_p}{\rho_{air}}\right) D^2\right] Cc \quad \text{(A26)}$$

where the linearized slip correction is given by:

$$Cc = 1.0 + 1.246(2\lambda/D) \quad \text{(A27)}$$

For a polydisperse aerosol, we average these quantities over the kth moment (M_k) of the size distribution $n(d_p)$ as follows [cf. *Kramm et al.*, 1992]:

$$\hat{X}_k = \frac{1}{M_k} \int_{-\infty}^{\infty} X D^k n(\ln D) d \ln D \quad \text{(A28)}$$

where $X = D_p$ or v_G. Substituting for D_p and v_G, performing the integrations assuming a lognormal size distribution, simplifying the algebra, and letting $Kn_g = 2\lambda/D_g$, we get

$$\hat{D}_{pk} = \tilde{D}_{pg}\left\{\exp\left(\frac{(-2k+1)}{2}\ln^2\sigma_g\right) + 1.246\, Kn_g \exp\left(\frac{(-4k+4)}{2}\ln^2\sigma_g\right)\right\} \quad \text{(A29)}$$

with

$$\tilde{D}_{pg} = \left(\frac{k_b T}{3\pi\nu\rho_{air} D_g}\right) \quad \text{(A30)}$$

for the polydisperse diffusivity, and

$$\hat{v}_{Gk} = \tilde{v}_{Gg}\left\{\exp\left(\frac{(4k+4)}{2}\ln^2\sigma_g\right) + 1.246\, Kn_g \exp\left(\frac{(2k+1)}{2}\ln^2\sigma_g\right)\right\} \quad \text{(A31)}$$

with

$$\bar{v}_{Gg} = \frac{g}{18\nu}\left(\frac{\rho_p}{\rho_{air}}\right) D_g^2 \qquad \text{(A32)}$$

for the polydisperse settling velocity. Note that for a monodisperse distribution ($\sigma_g = 1.0$), we recover the correct forms for the diffusivity and settling velocity including the slip corrections. The deposition velocity for the kth moment of a polydisperse aerosol is then given by

$$\hat{v}_{dk} = (r_a + \hat{r}_{dk} + r_a\hat{r}_{dk}\hat{v}_{Gk})^{-1} + \hat{v}_{Gk} \qquad \text{(A33)}$$

which is a generalization of a form obtained independently by *Slinn and Slinn* [1980] and *Pleim et al.* [1984]. The surface layer resistance is given by

$$\hat{r}_{dk} = \left\{ (Sc_k^{-2/3} + 10^{-3/St_k})\left(1 + 0.24\,\frac{w_*^2}{u_*^2}\right) u_* \right\}^{-1} \qquad \text{(A34)}$$

where the Schmidt and Stokes numbers are given by $Sc_k = \nu/\hat{D}_{pk}$ and $St_k = (u_*^2/g\nu)\hat{v}_{Gk}$, respectively. The form for the surface layer resistance is well known [e.g., *Seinfeld*, 1986; *Slinn*, 1982] except for the facter involving the convective velocity scale, w_*, an empirical correction obtained by *Wesely et al.* [1985] who approximated the factor involving the Schmidt and Stokes numbers by a constant of 0.002.

When treating multimodal aerosol distributions, we must consider the values of $\hat{v}_{dk}$ described above as determined for each mode. Assuming that particle density is not a function of size and is the same for each mode, we can define the deposition velocity for total particle moment as a weighted average over both modes, and we have equation (13)

$$v_{dk} = \frac{M_{ki}\hat{v}_{dki} + M_{kj}\hat{v}_{dkj}}{M_{ki} + M_{kj}} \qquad k = 0, 3$$

A4. Prediction Cycle

Particle number concentration ($k = 0$) is predicted using (5). New particle production rates are represented by E_{0i} and E_{0j}. This includes emissions for both modes and nucleation only in the i mode. The species mass (e.g., sulfate and ammonia) is predicted using (1). Total particle volume is constructed using the sulfate and ammonium (derived from the ammonia), water, any other additional species, and appropriate densities. The number concentration, diameters, and standard deviations determine the third moment fraction in each mode. The total particle volume then is converted to third moment by dividing by (π/6) and the third and sixth moments constructed for each mode. Equations (5) are solved without the transport terms for $k = 3$ and $k = 6$. New diameters and standard deviations then can be calculated and the cycle advanced. If the standard deviations are fixed, the sixth moments are not calculated.

A5. Computational Details

The advection algorithms are identical to RADM (i.e., the *Smolarkiewicz* [1984] scheme). The advection time step in this implementation is 900 s. Calculations done by *Whitby et al.* [1991] confirm that the aerosol dynamics algorithms are robust enough at this time step. We recognize that nucleation bursts happen at short timescales; but the smoothed hourly plots given by *Easter and Peters* [1994] suggest that our parameterization of nucleation is compatible with this time step.

Notation

A_{wl} aqueous production rate of species l, ppm s^{-1}.
$\bar{c}$ kinetic velocity of vapor molecules, equal to $(8\mathbf{R}T/\pi m_w)^{1/2}$.
C_l molar mixing ratio of species l, ppm.
$\dot{C}_l$ total rate of change of concentration of species l, ppm s^{-1}.
C_{kij}, C_{kji} intermodal coagulation rate, μm^k cm^{-3} s^{-1}.
C_{kii}, C_{kjj} intramodal coagulation rate, μm^k cm^{-3} s^{-1}.
$\hat{C}^{fm}_{kij}$, $\hat{C}^{fm}_{kbb}$ intermodal and intramodal coagulation rates for the free-molecular size range, μm^k cm^{-3} s^{-1}.
C_{crit} critical concentration for production of new particles (see appendix for details), μg m^{-3}.
C_{ss} steady state concentration for condensation on existing particles (see appendix for details), μg m^{-3}.
$\hat{C}^{nc}_{kij}$, $\hat{C}^{nc}_{kbb}$ intermodal and intramodal coagulation rates for the near-continuum size range, μm^k cm^{-3} s^{-1}.
D particle diameter, μm.
D_g geometric mean particle diameter for lognormal size distribution, μm.
D_v vapor diffusivity, cm^2 s^{-1}.
D_p particle diffusivity, cm^2 s^{-1}.
D_{wl} wet deposition loss rate of species l, ppm s^{-1}.
E_l emissions rate for species l, ppm s^{-1}.
E_{ki}, E_{kj} emissions rates for moment k of modes i and j, respectively, μm^k cm^{-3} s^{-1}.
G_{ki}, G_{kj} mean condensational growth rates for moment k of modes i and j, respectively, μm^k cm^{-3} s^{-1}.
$\hat{I}_{ki}$, $\hat{I}_{kj}$ integrals which contribute to mean condensational growth rates (see appendix for details), μm^k cm^{-3} s^{-1}.
L_l loss rate of species l due to gas phase chemical reaction, s^{-1}.
LWC liquid water content of aerosol particles, μg m^{-3}.
M_k kth moment of the number distribution, μm^k cm^{-3}.
M_{ki}, M_{kj} kth moment of the number distribution for modes i and j, respectively, μm^k cm^{-3}.
$\dot{M}_k$ total rate of change of the kth moment of the number distribution, μm^k cm^{-3} s^{-1}.
m_w molecular weight, cm s^{-1}.
$n(\ln D)$ distribution function for the number concentration of aerosol particles, cm^{-3} μm^{-1}.
N total number concentration of aerosol particles, cm^{-3}.
$\dot{N}$ time rate of change of the total number concentrations of aerosol particles, cm^3 s^{-1}.
p_s saturation vapor pressure of condensing species, atm.
P^* $P_{sfc} - P_{top}$, mbar.
P_{sfc} surface pressure, mbar.
P_{top} pressure at model top (100 mbar), mbar.
P_l production rate of species l due to gas-phase chemical reaction, ppm s^{-1}.
R_l ratio of molecular weight of species l to molecular weight of air.
$\mathbf{R}$ gas constant, J °K^{-1} mol^{-1}.
S_v saturation ratio of condensing species.
$\mathbf{V}$ horizontal wind velocity, m s^{-1}.
v_{dk} particle deposition velocity for kth moment, cm s^{-1}.
v_G particle settling velocity, cm s^{-1}.
α accommodation coefficient.
λ mean free path of air, cm.
ν kinematic viscosity of air, cm^2 s^{-1}.

ρ_l density of species l, g cm^{-3}.
ρ_p density of particles, g cm^{-3}.
ρ_{air} density of air, g cm^{-3}.
σ $(P - P_{top})/P^*$.
$\dot{\sigma}$ time rate of change of σ, s^{-1}.
σ_g geometric standard deviation of lognormal size distribution.
$\psi(D)$ size-dependent portion of growth law, m^3 s^{-1}.
Ψ_T size-independent portion of growth law.
Ω_i, Ω_j partition coefficients for condensational growth of i and j modes (see appendix for details).

Acknowledgments. The authors wish to thank Jason K. S. Ching and Adel Hanna for their encouragement and support during this project. We also wish to thank Sonia Kreidenweis for her comments and advice. We wish to express our appreciation to Julius Chang and Mark Beauharnois for providing the data for Figure 2 and to Kiran Alapaty for his assistance with the supercomputer implementation of the aerosol version of TSEM. All computation for this work was done at and with the support of the National Environmental Supercomputer Center of the U.S. EPA at Bay City, Michigan. The information in this document has been funded wholly by the United States Environmental Protection Agency and has been subjected to Agency review and approved for publication. Mention of trade names or commercial products does not constitute an endorsement or recommendation for use.

References

Aurian-Blajeni, B., J. M. Wolfson, and P. Koutrakis, Measurement of partial vapor pressure of ammonia over acid ammonium sulfate solutions by an integral method, paper presented at Eleventh Annual Meeting, Am. Assoc. for Aerosol Res., San Francisco, Calif., Oct. 12–16, 1992.

Binkowski, F. S., and K. Alapaty, Performance of a prototype regional particulate model, paper EUROTRAC Workshop on Regional and Global Modeling of Minor Atmospheric Constituents, XVI General Assembly, Eur. Geophys. Soc., Wiesbaden, Germany, April 23–26, 1991.

Binkowski, F. S., and U. Shankar, Atmospheric aerosol size distributions and the Clean Air Act, paper presented at the 13th International Meeting on Nucleation and Atmospheric Aerosols, Comm. on Nucleation and Aerosols, Salt Lake City, Utah, Aug. 24–28, 1992a.

Binkowski, F. S., and U. Shankar, Model predictions of aerosol optical characteristics responding to humidity and emissions changes, paper presented at the Conference on Visibility and Fine Particles, Univ. of Vienna, Vienna, Austria, Sept. 15–18, 1992b.

Binkowski, F. S., and U. Shankar, Model predictions of aerosol characteristics in industrial source regions and rural areas. paper presented at the 11th Annual Meeting, Am. Assoc. for Aerosol Res., San Francisco, Calif., Oct. 12–16, 1992c.

Binkowski, F. S., and U. Shankar, Development of an algorithm for the interaction of a distribution of aerosol particles with cloud water for use in a three-dimensional Eulerian air quality model. paper presented at Fourth International Aerosol Conference, Am. Assoc. for Aerosol Res., Los Angeles, Calif., Aug. 29–Sept., 2, 1994.

Binkowski, F. S., J. S. Chang, R. L. Dennis, S. Reynolds, P. J. Samson, and J. D. Shannon, Regional acid deposition modeling, NAPAP SOS/T Report 3, in *National Acid Precipitation Assessment Program, Acidic Deposition: State of Science and Technology*, vol. I, pp. 3-1–3-59, U.S. Govt. Print. Off., Washington, D. C., 1990.

Byun, D. W., On the analytical solutions of flux-profile relationships for the atmospheric boundary layer, *J. Appl. Meteorol.*, *29*, 652–657, 1990.

Byun, D. W., Determination of similarity functions of the resistance laws for the planetary boundary layer using surface-layer similarity functions, *Boundary Layer Meteorol.*, *57*, 17–48, 1991.

Byun, D. W., and F. S. Binkowski, Sensitivity of RADM to point source emissions processing, in *Proceedings of the Seventh AMS Joint Conference on Applications of Air Pollution Meteorology with AWMA*, pp. 70–73, Am. Meteorol. Soc., Boston, Mass., 1991.

Chang, J. S., R. A. Brost, I. S. A. Isaksen, S. Madronich, P. Middleton, W. R. Stockwell, and C. J. Walcek, A three-dimensional Eulerian acid deposition model: Physical concepts and formulation, *J. Geophys. Res.*, *92*, 14,681–14,700, 1987.

Chang, J. S., et al., The regional acid deposition model and engineering model, NAPAP SOS/T Report 4, in *National Acid Precipitation Assessment Program, Acidic Deposition: State of Science and Technology*, vol. I, pp. 4-1–4-F42, U.S. Govt. Print. Off., Washington, D. C., 1990.

Chaumerliac, N., Evaluation des termes de captation dynamique dans un modèle tridimensionnel à mésoéchelle de lessivage de l'atmosphère, thèse, Univ. de Clermont II, Clermont, France, 1984.

Chaumerliac, N., E. C. Nickerson, and R. Rosset, A 3D mesoscale model as a potential tool for evaluation of sulfate particles scavenging, *Ann. Geophys., Ser. B*, *4*(3), 345–352, 1986.

Ching, J. K. S., and F. S. Binkowski, Modeling the deposition of semi-volatile air toxic pollutants to the Great Lakes using a regional scale particulate model, paper presented at the Eleventh Annual Meeting, Am. Assoc. for Aerosol Res., San Francisco, Calif., Oct. 12–16, 1992.

Clegg, S. L., and P. Brimblecombe, Solubility of ammonia in pure aqueous and multicomponent solutions, *J. Phys. Chem.*, *93*, 7237–7248, 1989.

Clegg, S. L., and K. S. Pitzer, Thermodynamics of multicomponent, miscible, ionic solutions, 1, Generalized equations for symmetrical electrolytes, *J. Phys. Chem.*, *96*, 3513–3520, 1992.

Clegg, S. L., K. S. Pitzer, and P. Brimblecombe, Thermodynamics of multicomponent, miscible, ionic solutions, 2, Mixtures including unsymmetrical electrolytes, *J. Phys. Chem.*, *96*, 9470–9479, 1992.

Cohen, M. D., R. C. Flagan, and J. H. Seinfeld, Studies of concentrated electrolyte solutions using the electrodynamic balance, 3, Solute nucleation, *J. Phys. Chem.*, *81*, 4583–4590, 1987.

Easter, R. C., and L. K. Peters, Binary homogeneous nucleation: temperature and relative humidity fluctuations and non-linearity, paper presented at Conference on Atmospheric Chemistry, Am. Meteorol. Soc., Anaheim, Calif., Jan. 17–22, 1993.

Easter, R. C., and L. K. Peters, Binary homogeneous nucleation: Temperature and relative humidity fluctuations, nonlinearity, and aspects of new particle production in the atmosphere, *J. Appl. Meteorol.*, *33*, 775–784, 1994.

Finlayson-Pitts, B. J., and J. N. Pitts Jr., *Atmospheric Chemistry: Fundamentals and Experimental Techniques*, John Wiley, New York, 1986.

Friedlander, S., *Smoke, Dust, and Haze: Fundamentals of Aerosol Behavior*, John Wiley, New York, 1977.

Giorgi, F., Development of an atmospheric aerosol model for studies of global budgets and effects of airborne particulate material, *GIT-NCAR coop. thesis 102*, Ga. Inst. of Technol., Atlanta, 1986.

Grosjean, D., and J. H. Seinfeld, Parameterization of the formation potential of secondary organic aerosols, *Atmos. Environ.*, *23*, 1733–1747, 1989.

Hänel, G., The properties of atmospheric aerosol particles as functions of the relative humidity at thermodynamic equilibrium with the surrounding air, *Adv. Geophys.*, *19*, 73–89, 1976.

Harrison, R. M., and A. M. N. Kitto, Estimation of the rate constant for the reaction of acid sulfate aerosol with NH_3 gas from atmospheric measurements, *J. Atmos. Chem.*, *15*, 133–143, 1992.

Hass, H., H. J. Jakobs, M. Memmesheimer, A. Ebel, and J. S. Chang, Simulation of a wet deposition case in Europe using the European Acid Deposition Model (EURAD), in *Air Pollution Modeling and Its Applications*, vol. 8, edited by H. van Dop and D. G. Steyn, pp. 205–213, Plenum, New York, 1991.

Jaecker-Voirol, A., and P. Mirabel, Heteromolecular nucleation in the sulfuric acid-water system, *Atmos. Environ.*, *23*, 2053–2057, 1989.

Kerminin, V.-M., and A. S. Wexler, Post-fog nucleation of H_2SO_4-H_2O particles in smog, *Atmos. Environ.*, *28*, 2399–2406, 1994.

Kötz, A., Bedeutung der Aerosole für den Ferntransport von Schadstoffen in der Troposphäre, Mitt. Inst. Geophys. Meteorol. Univ. *Koeln*, *81*, 1991.

Kötz, A., M. Memmesheimer, A. Ebel, and H. Hass, Modelling of the aerosol phase in the European Regional Acid Deposition Model (EURAD), paper presented at EUROTRAC Workshop on Regional and Global Modelling of Minor Atmospheric Constituents, XVI General Assembly, Eur. Geophys. Soc., Wiesbaden, Germany, April 23–26, 1991.

Koutrakis, P., and B. Aurian-Blajeni, Measurement of partial vapor pressure of ammonia over a acid ammonium sulfate solutions by an integral method, *J. Geophys. Res.*, *98*, 2941–2948, 1993.

Kramm, G., K. D. Beheng, and H. Müller, Modeling of the vertical transport of polydispersed aerosol particles in the atmospheric surface layer, in *Precipitation Scavenging and Atmospheric Surface Exchange*, vol. 1, edited by S. E. Schwartz and W. G. N. Slinn, pp. 1125–1141, Hemisphere, Bristol, Pa., 1992.

McElroy, M. W., R. C. Carr, D. S. Ensor, and G. R. Markowski, Size distribution of fine particles from coal combustion, *Science*, *215*, 13–19, 1982.

McHenry, J. N., F. S. Binkowski, R. L. Dennis, J. S. Chang, and D. Hopkins, The Tagged Species Engineering Model (TSEM), *Atmos. Environ., Part A*, *26*, 1427–1443, 1992.

Middleton, P. B., Denver Air Quality Modeling Study (DAQMS), paper presented at Twelfth Annual Meeting, Am. Assoc. for Aerosol Res., Oak Brook, Ill., Oct. 11–15, 1993.

Middleton, P. B., and C. S. Kiang, A kinetic model for the formation and growth of secondary sulfuric acid particles, *J. Aerosol Sci.*, *9*, 359–385, 1978.

Nair, P. V. N., and K. G. Vohra, Growth of aqueous sulphuric acid droplets as a function of relative humidity, *J. Aerosol Sci.*, *6*, 265–271, 1975.

Pandis, S. N., R. A. Harley, G. R. Cass, and J. H. Seinfeld, Secondary organic aerosol formation and transport, *Atmos. Environ., Part A*, *26*, 2269–2282, 1992.

Pankow, J. F., Review and comparative analysis of the theories on partitioning between the gas and aerosol particulate phases in the atmosphere, *Atmos. Environ.*, *21*, 2275–2283, 1987.

Pilinis, C., and J. H. Seinfeld, Continued development of a general equilibrium model for inorganic multicomponent atmospheric aerosols, *Atmos. Environ.*, *21*, 2453–2466, 1987.

Pilinis, C., J. H. Seinfeld, and D. Grosjean, Water content of atmospheric aerosols, *Atmos. Environ.*, *23*, 1601–1606, 1989.

Pitzer, K. S., Thermodynamic model for aqueous solution of liquid-like density, *Rev. Mineral.*, *17*, 97–142, 1987.

Pitzer, K. S., Ion interaction approach: Theory and data correlation, in *Activity Coefficients in Electrolyte Solutions*, edited by K. S. Pitzer, pp. 75–154, CRC Press, Boca Raton, Fla., 1991.

Placet, M., et al., Emissions involved in acidic deposition processes, NAPAP SOS/T Report 1, in *National Acid Precipitation Assessment Program, Acidic Deposition: State of Science and Technology*, vol. I, pp. 1-1–1-183, U.S. Govt. Print. Off., Washington, D. C., 1990.

Pleim, J. E., and J. S. Chang, A non-local closure model for vertical mixing in the convective boundary layer, *Atmos. Environ., Part A*, *26*, 965–981, 1991.

Pleim, J. E., A. Venkatram, and R. Yamartino, *ADOM/TADAP Model Development Program*, vol. 4, *The Dry Deposition Module*, Ont. Min. of the Environ., Rexdale, Canada, 1984.

Pratsinis, S. E., Simultaneous aerosol nucleation, condensation, and coagulation in aerosol reactors, *J. Colloid Interface Sci.*, *124*, 417–427, 1988.

Pruppacher, H. R., and J. D. Klett, *Microphysics of Clouds and Precipitation*, D. Reidel, Norwell, Mass., 1978.

Richardson, C. B., and J. F. Spann, Measurement of the water cycle in a levitated ammonium sulfate particle, *Atmos. Environ.*, *15*, 563–571, 1991.

Rood, M. J., M. A. Shaw, T. V. Larson, and D. S. Covert, Ubiquitous nature of ambient metastable aerosol, *Nature*, *337*, 537–539, 1989.

Russell, A. G., G. J. McRae, and G. R. Cass, Mathematical modeling of the formation and transport of ammonium nitrate aerosol, *Atmos. Environ.*, *17*, 949–964, 1983.

Russell, A. G., G. J. McRae, and G. R. Cass, The dynamics of nitric acid production and the fate of nitrogen oxides, *Atmos. Environ.*, *19*, 893–903, 1985.

Saxena, P., A. B. Hudischewskyj, C. Seigneur, and J. H. Seinfeld, A comparative study of equilibrium approaches to the chemical characterization of secondary aerosols, *Atmos. Environ.*, *20*, 1471–1483, 1986.

Seinfeld, J. H., *Atmospheric Chemistry and Physics of Air Pollution*, John Wiley, New York, 1986.

Shankar, U., and F. S. Binkowski, The EPA/NOAA Regional Particulate Model, A three-dimensional chemical and transport model for gases and aerosols, paper presented at the 13th International Meeting on Nucleation and Atmospheric Aerosols, Comm. on Nucleation and Aerosols, Salt Lake City, Utah, Aug. 24–28, 1992.

Shankar, U., and F. S. Binkowski, Sulfate wet depostion in a three-dimensional Eulerian air quality modeling framework, paper presented at Fourth International Aerosol Conference, Am. Assoc. for Aerosol Res., Los Angeles, Calif., Aug. 29–Sept. 2, 1994.

Slinn, W. G. N., Rate-limiting aspects of in-cloud scavenging, *J. Atmos. Sci.*, *31*, 1172–1173, 1974.

Slinn, W. G. N., Prediction for particle deposition to vegatative canopies, *Atmos. Environ.*, *16*, 1785–1794, 1982.

Slinn, S. A., and W. G. N. Slinn, Prediction for particle deposition on natural waters, *Atmos. Environ.*, *14*, 1013–1016, 1980.

Smolarkiewicz, P. K., A fully multidimensional positive-definite advection scheme with small implicit diffusion. *J. Comput. Phys.*, *54*, 325–362, 1984.

Spann, J. F., and C. B. Richardson, Measurement of the water cycle in mixed ammonium acid sulfate particles, *Atmos. Environ.*, *19*, 819–825, 1985.

Stauffer, D. R., and N. L. Seaman, Use of four-dimensional data assimilation in a limited area mesoscale model, I, Experiments with synoptic scale data, *Mon. Weather Rev.*, *118*, 1250–1277, 1990.

Stauffer, D. R., N. L. Seaman, and F. S. Binkowski, Use of four-dimensional data assimilation in a limited area mesoscale model, II, Effects of data assimilation within the planetary boundary layer, *Mon. Weather Rev.*, *119*, 734–754, 1991.

Tang, I. N., On the equilibrium partial pressures of nitric acid and ammonia in the atmosphere, *Atmos. Environ.*, *14*, 819–828, 1980.

Tang, I. N., and H. R. Munkelwitz, Aerosol growth studies, III, Ammonium bisulfate aerosols in a moist atmosphere, *J. Aerosol Sci.*, *8*, 321–330, 1977.

Toon, O. B., R. P. Turco, D. Westphal, R. Malone, and M. S. Liu, A multidimensional model for aerosols: Description of computational analogs, *J. Atmos. Sci.*, *45*, 2123–2143, 1988.

Twomey, S., *Atmospheric Aerosols*, Elsevier, New York, 1977.

Van Dingenen, R., and F. Raes, Determination of the condensation accommodation coefficient of sulfuric acid on water-sulfuric acid aerosol, *Aerosol Sci. Technol.*, *15*, 93–106, 1991.

Warneck, P., *Chemistry of the Natural Atmosphere*, Academic, San Diego, Calif., 1988.

Wesely, M. L., D. R. Cook, R. L. Hart, and R. E. Speer, Measurement and parameterization of particulate sulfur dry deposition over grass, *J. Geophys. Res.*, *90*, 2131–2143, 1985.

Westphal, D., O. B. Toon, and T. N. Carlson, A case study of mobilization and transport of Saharan dust, *J. Atmos. Sci.*, *45*, 2145–2175, 1988.

Wexler, A. S., and J. H. Seinfeld, Second-generation inorganic aerosol model, *Atmos. Envion., Part A*, *25*, 2731–2748, 1991.

Wexler, A. S., F. W. Lurmann, and J. H. Seinfeld, Modeling urban and regional aerosols, I, Model development, *Atmos. Environ.*, *28*, 531–546, 1994.

Whitby, K. T., The physical characteristics of sulfur aerosols, *Atmos. Environ.*, *12*, 135–159, 1978.

Whitby, E. R., P. H. McMurry, U. Shankar, and F. S. Binkowski, *Modal Aerosol Dynamics Modeling*, *Rep. 600/3-91/020*, Atmos. Res. and Exposure Assess. Lab., U.S. Environ. Prot. Agency, Research Triangle Park, N. C., 1991. (Available as NTIS PB91-161729/AS from Natl. Tech. Inf. Serv., Springfield, Va.).

F. S. Binkowski, Atmospheric Sciences Modeling Division, Air Resources Laboratory, Mail Drop 80, National Oceanic and Atmospheric Administration, Research Triangle Park, NC 27711. (e-mail: fzb@hpcc.epa.gov)

U. Shankar, MCNC, P. O. Box 12889, Research Triangle Park, NC 27709-2889.

(Received October 12, 1993; revised April 14, 1995; accepted June 29, 1995.)